Hydrol. Earth Syst. Sci., 29, 6479–6498, 2025 https://doi.org/10.5194/hess-29-6479-2025 © Author(s) 2025. This work is distributed under the Creative Commons Attribution 4.0 License.





The influence of a rock glacier on the riverbed hydrological system

Bastien Charonnat^{1,2,3}, Michel Baraer^{1,2,3}, Eole Valence⁴, Janie Masse-Dufresne^{1,2,3}, Chloé Monty⁵, Kaiyuan Wang⁶, Elise Devoie⁷, and Jeffrey M. McKenzie⁴

Correspondence: Bastien Charonnat (bastien.charonnat.1@ens.etsmtl.ca)

Received: 11 January 2025 – Discussion started: 20 February 2025

Revised: 25 September 2025 – Accepted: 17 October 2025 – Published: 19 November 2025

Abstract. Climate change is accelerating cryosphere degradation in mountain regions, and altering hydrological and geomorphological dynamics within deglaciating catchments. Rock glaciers, which degrade slower than glaciers, can exert a prolonged influence on water resources in alpine watersheds. This study investigates both the direct and indirect influences of a rock glacier on the Shár Shaw Tagà (Grizzly Creek) riverbed in the St. Elias Mountains (Yukon, Canada). We applied a unique multimethod approach combining hydro-physicochemical and isotopic characterization, drone-based thermal infrared (TIR) imagery, and visible time-lapse imagery.

Results reveal that the rock glacier's geomorphic and thermal properties constrain the riverbed and its underlying alluvial aquifer, driving shallow groundwater resurgence. These indirect disruptions promote downstream cryo-hydrological processes by facilitating aufeis formation and modifying the physicochemical properties of surface water. In contrast, direct hydrological influence from the rock glacier's internal drainage system to downstream surface waters appears minimal. This configuration is transitional, as the constraint imposed by ground ice is expected to diminish with progressive permafrost degradation.

Overall, this study identifies the critical yet transient role of rock glaciers in alpine hydrology. Beyond their internal hydrological behaviour, they shape catchment hydrology through geomorphic controls. Our findings highlight the need to account for indirect effects when evaluating hydrological dynamics in deglaciating catchments.

1 Introduction

Climate change is profoundly transforming mountain regions, where the cryosphere has a critical role in regulating water resources that sustain downstream ecosystems and communities. With rising global temperatures, high mountain areas are experiencing accelerated deglaciation, characterized by glacial retreat and permafrost thaw (Hock et al., 2019). These processes drive rapid geomorphological and hydrological reconfigurations in proglacial systems (Carrivick and Heckmann, 2017). Understanding how cryosphere degradation affects mountain hydrology and hydrogeology is therefore essential for predicting future water availability (Hayashi, 2020; van Tiel et al., 2024).

Among cryospheric features, rock glaciers degrade the slowest, continuing to influence hydrology long after glaciers have retreated (Bolch and Marchenko, 2009; Harrison et al., 2021; Jones et al., 2021). Rock glaciers are tongue-shaped landforms composed of rocky debris and ice, which creep due to the deformation of the ice-debris matrix, concentrated in the shear horizon (Arenson et al., 2002). They are commonly found in high mountain environments and oc-

¹Hydrology, Climate and Climate Change laboratory – École de technologie supérieure (ÉTS), Montreal, Quebec, Canada

²GEOTOP (Research Centre on the Dynamics of the Earth System), Montreal, Quebec, Canada

³CentrEau (Ouebec Research Water Centre), Ouebec City, Ouebec, Canada

⁴Department of Earth and Planetary Science – McGill University, Montreal, Quebec, Canada

⁵Department of Earth Sciences – Simon Fraser University, Burnaby, British Columbia, Canada

⁶Department of Earth, Environmental & Planetary Sciences – Brown University, Providence, Rhode Island, United States

⁷Civil Engineering department – Queen's University, Kingston, Ontario, Canada

cur in both discontinuous and continuous permafrost zones (Barsch, 1996).

Historically, research on rock glaciers has focused primarily on two aspects: their hydrological behaviour, particularly their direct influence on catchment hydrology, and their geomorphological dynamics. In this study, we differentiate between direct hydrological influence (i.e., related to rock glacier internal hydrological processes and resulting outflows) and indirect hydrological influence (i.e., arising from external processes linked to rock glacier dynamics, such as geomorphic obstruction of a riverbed, limiting hydraulic conductivity and potentially altering surface and shallow groundwater flow patterns).

Direct hydrological influence of rock glaciers involves buffering catchment surface water discharge, by sustaining baseflow and attenuating discharge response to intense precipitation peaks (Bearzot et al., 2023; Reato et al., 2022; Wagner et al., 2021). A rock glacier's hydrological behaviour is closely tied to its internal distribution of frozen and liquid water (Harrington et al., 2018; Wagner et al., 2016; Winkler et al., 2016). Unfrozen layers in summer can act as reservoirs and conduits for water flow (Halla et al., 2021; Harrington et al., 2018; Navarro et al., 2023; Wagner et al., 2020). In addition to liquid water, intact rock glaciers (i.e., containing frozen content) store significant volumes of solid water as interstitial or massive ice (Chakravarti et al., 2022; Halla et al., 2021; Jones et al., 2018; Wagner et al., 2021). However, internal ice melt typically contributes only minimally to total rock glacier discharge (Arenson et al., 2022). Rock glaciers also directly influence downstream water quality by increasing solute concentrations (Colombo et al., 2018; Colombo et al., 2019; Schreder et al., 2023; Engel et al., 2019; Wanner et al., 2023; Zarroca et al., 2021) and cooling stream temperatures (Bearzot et al., 2023; Brighenti et al., 2019; Colombo et al., 2020).

In addition, rock glaciers can exert indirect hydrological effects, as they are dynamic landforms that may advance, constrain, or even dam riverbeds. Such effects have been reported in High Asia (Blöthe et al., 2019; Falatkova et al., 2020; Hewitt, 2014) and the Alps (Colombo et al., 2020). Furthermore, topographic changes driven by glacial retreat and paraglacial processes can force channel confinement (Marren and Toomath, 2014). Climate change has intensified rock glacier movement (Delaloye et al., 2010; Kummert et al., 2021; PERMOS, 2019), sometimes causing destabilization (Marcer et al., 2021) and channel disruption (Sorg et al., 2015). Additionally, sudden mass movements, such as the catastrophic collapse of rock glacier lobes, have triggered debris flows with downstream geomorphic impacts (Bodin et al., 2015; Scotti et al., 2017). Riverbeds and outwash plains play an important role in sustaining baseflow and aquatic habitats (Käser and Hunkeler, 2016; Müller et al., 2024). However, to our knowledge, the indirect hydrological effects of rock glacier dynamics have not yet been assessed or compared with the direct effects of rock glaciers.

The objective of this study is to address this research gap by simultaneously examining the direct and indirect hydrological influences of a rock glacier extending into a valley floor. Specifically, we aim to elucidate the underlying processes and anticipate the potential evolution of the system. We focus on surface water and shallow groundwater fluxes within a section of the Shár Shaw Tagà River in the St. Elias Mountains, Yukon, Canada, where the riverbed is constrained by the rock glacier. To reach this objective, we use a multimethod approach that combines observational techniques and natural tracer analyses in two steps:

- Monitoring and surveying of groundwater exfiltration, hypothesized to occur within the constrained river section, and causing significant outflows and winter aufeis formation. To assess the presence of important groundwater outflows in this section, we use drone-based thermal infrared (TIR) surveys, time-lapse camera (TLC) monitoring and radon activities measurements.
- Physico-hydrochemical characterization to distinguish outflows associated with either the direct or the indirect influences of the rock glacier. We use synoptic sampling and hydrochemical analyses to characterize distinct water sources and their relative contributions.

The novelty of this research lies in its simultaneous assessment of direct and indirect hydrological influences of a rock glacier on catchment hydrology. Our findings highlight the complex and dynamic role of rock glaciers in alpine catchment systems and provide insights applicable to similar environments worldwide.

2 Study site

Shár Shaw Tagà, meaning Grizzly Creek in the Southern Tutchone indigenous language, is a $32 \,\mathrm{km^2}$ glacierized catchment located within the traditional lands of the Kluane First Nation and the White River First Nation (Fig. 1a). It is within the Kluane National Park and Reserve in the St. Elias Mountains, southwestern Yukon Territory, Canada $(61^\circ05'13''\,\mathrm{N}, 139^\circ07'18''\,\mathrm{W})$. The eastern flank of the St. Elias Mountains experiences a dry subarctic climate, characterized by annual precipitation ranging from 300 to 500 mm yr $^{-1}$ and a mean annual temperature between -8 and $-12\,^\circ\mathrm{C}$ (Wahl et al., 1987).

Publications prior to 2024 referred to the area by the toponym "Grizzly Creek" rather than Shár Shaw Tagà. The upper Shár Shaw Tagà catchment (Fig. 1b) contains eight glaciers, the largest of which is G-A1, covering an area of 3.2 km². Due to its heavily fractured bedrock lithology and steep slopes, the valley is characterized by significant mass wasting processes and depositional features, including nine previously identified rock glaciers (Johnson, 1978; Evin et al., 1997). Of these nine rock glaciers, seven extend into the

riverbed along the valley floor, with some exerting considerable geomorphological constraints on the stream.

The present study focuses on the RG-A1 rock glacier, located on the western side of the upper Shár Shaw Tagà valley. The front of RG-A1 advances in the valley, constraining the Shár Shaw Tagà River against the opposing talus slope. RG-A1 spans elevations between 1700 and 1850 m a.s.l. The southern lobes of RG-A1 appear older, characterized by vegetation cover and a smoother frontal morphology, while the northern lobes are younger, with sparse or absent vegetation, sharper forms, and a steeper front (Johnson, 1978). Based on geophysical surveys, Evin et al. (1997) report a 20 to 40 m thick frozen layer as well as the presence of massive ice lenses at depth in RG-A1.

The outwash plains upstream and downstream of RG-A1 are separated by a "narrow section" of the Shár Shaw Tagà River, which can be divided into two subsections: N1 and N2 (Fig. 2). N1 extends from the outlet of the upstream outwash plain to a bedrock outcrop visible on the opposite talus slope to RG-A1. N2 extends from this bedrock outcrop to the outlet of the "narrow section", where the river reaches the downstream outwash plain. Although previous studies did not classify the talus slope opposed to RG-A1 as a rock glacier, it is suspected to be a protalus rampart (or small active rock glacier) based on environmental and topographic criteria outlined in Scapozza (2015). We noted the absence of an upstream permanent snow field, the presence of coarse boulders in the upslope area, a steep front with exposed fine sediments, and a juxtaposition and superimposition to other rock glaciers.

In 1974, Johnson (1978) observed that meltwater drained into a sinkhole located in the rooting zone of RG-A1 (at approximately 1850 m a.s.l.), with no major resurgence observed at its front (at 1700 m a.s.l.). In 1975, a new sinkhole was observed upstream of the first one, and a significant resurgence was reported on the northern part of RG-A1. Dry channels on the surface of RG-A1 in 1975 were interpreted by Johnson as abandoned surface drainage pathways, highlighting the dynamic and variable hydrological behaviour of RG-A1. Field observations by our team from 2018 to 2023 indicate no significant visible outlet from the rock glacier, despite its position downstream of an 8 km² subcatchment containing the G-B1 and G-B2 glaciers. The only visible outlets consist of low-discharge springs around the RG-A1 front, particularly concentrated along the N1 subsection. The lack of surface outflow from the rock glacier suggests subsurface connectivity with the Shár Shaw Tagà River.

During low-discharge periods, such as in June 2023, we observed infiltration of Shár Shaw Tagà River water into the riverbed, leaving the channel dry before the outwash plain upstream of RG-A1. Flow re-emerged in the N1 subsection, close to the rock glacier's front, visually sustained by springs and seepage. Additional subsurface flow paths are evident in winter through aufeis formation in the downstream outwash plain, documented by field observations since 2018 and on

satellite imagery, while no aufeis has been detected upstream between 2018 and 2023. Aufeis (or icings) are layered ice accumulations that develop when groundwater outflows persist under sub-zero temperatures (Ensom et al., 2020).

The configuration of RG-A1, which constrains the riverbed, together with these groundwater observations in the "narrow section", supports our hypothesis that the rock glacier exerts both direct and indirect hydrological influence on the riverbed system. Accordingly, our methodology focuses on characterizing the sources and impacts of groundwater exfiltration in this section.

3 Methods

3.1 Monitoring and surveying of groundwater exfiltration

3.1.1 TIR survey

Aerial and handheld thermal infrared (TIR) devices have been demonstrated as effective tools for mapping groundwater discharge into streams (Toran, 2019). Specifically, drone-based TIR technology allows for high spatial resolution observations of surface water—groundwater interactions (Vélez-Nicolás et al., 2021). Two common approaches for TIR surveys were considered: (1) generating stream temperature maps using high-definition TIR image orthomosaics from overlapping images (e.g., Abolt et al., 2018; Casas-Mulet et al., 2020; Rautio et al., 2015), and (2) using TIR videos or real-time scans (handheld or drone-based) to visualize mixing plumes and record GPS coordinates of observed points (e.g., Barclay et al., 2022; Briggs et al., 2016; Iwasaki et al., 2023).

Georeferenced thermal maps provide mesoscale coverage but require stable flying conditions, ground control points, and extensive post-processing (Webb et al., 2008). In contrast, TIR video or live scans enable real-time visualization of mixing dynamics at smaller scales (Antonelli et al., 2017). To identify and characterize cold groundwater emergence zones, we adopted the TIR video approach, which relies on relative temperature contrasts between stream water and suspected groundwater inflows rather than precise absolute temperatures. Previous studies have demonstrated that TIR video effectively highlights such contrasts even without embedded temperature scales (Antonelli et al., 2017; Briggs et al., 2016; Iwasaki et al., 2023, 2024). Drone-based TIR video surveys were conducted on 28 June 2024, between 08:00 and 10:00 LT, to maximize the coverage of shaded sections of the stream. The surveys were conducted using a DJI Mavic 3T Enterprise, equipped with a DJI RTK module and a DJI D-RTK 2 mobile station for GNSS base-station support. The Mavic 3T features a 48-megapixel RGB camera with a 24 mm focal length and a 640×512 -pixel thermal camera with a 40 mm focal length. The drone was manually con-

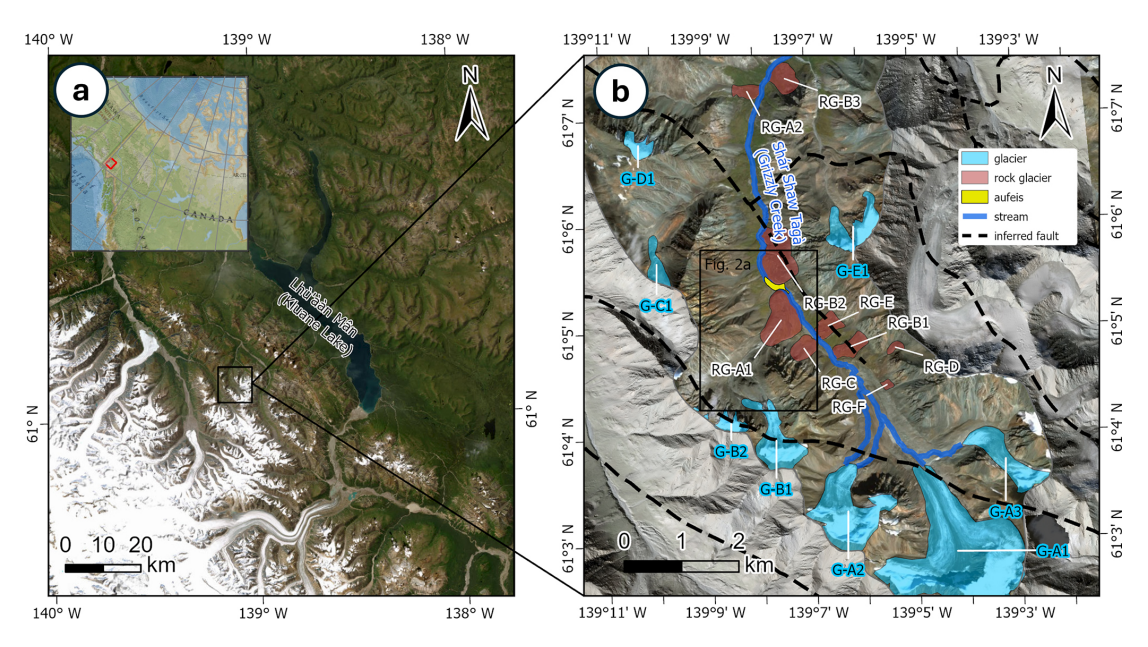


Figure 1. (a) Overview map showing the location of the Shár Shaw Tagà valley in southwestern Yukon, Canada. (b) Enlarged view of the study area from panel (a), highlighting key geomorphological features. The black frame outlines the extent of the map shown in Fig. 2a. ArcticDEM data: Polar Geospatial Center (Porter et al., 2023). Geological data: Dodds and Campbell (1992). Basemap credits: Esri.

trolled to optimize the capture of surface temperatures across wide sections of the Shár Shaw Tagà River, recording both TIR and RGB videos simultaneously. Flight altitudes ranged from 5 to 20 m above ground level with near-nadir angles to reduce geometric distortion and minimize emissivity-related error (Torgersen et al., 2001; Dugdale, 2016). The survey began 180 m upstream of the N1 subsection and ended 800 m downstream of the N2 subsection (Fig. 2).

The TIR video was visually analyzed to identify cold water emergence zones using two criteria: (1) a clear contrast between the dominant stream surface temperature and the suspected exfiltration area, with an area larger than $10\,\mathrm{cm^2}$, and (2) the presence of a turbulent mixing zone at least 1 m in length immediately downstream of the suspected area (flight data and information are available as supplemental material in Charonnat and Baraer, 2025). Absolute temperatures were not derived due to the absence of a calibrated color scale in the TIR video; instead, detection relied on qualitative identification of relative temperature differences appearing as visual color contrasts in the TIR video – typically, colder areas appeared as blue-toned patches compared to the green-toned stream and red-toned sunlit boulders.

When both criteria were met, the RGB video was used for confirmation. The Shár Shaw Tagà River, originating from glacial melt, has a substantial suspended sediment load, whereas groundwater is nearly free of suspended sediments. This contrast is visible in the RGB video frames. The observed thermal contrasts were consistent with previously measured field temperature differences between springs and stream water, typically < 2 and $< 6\,^{\circ}\text{C}$ (Table S1 in the Supplement) and exceeded the uncertainty range of uncorrected

thermal imagery under field conditions (Zappa et al., 1998). Finally, images of confirmed cold-water emergence zones were extracted from the videos for size evaluation.

3.1.2 TLC monitoring

Three RGB time-lapse cameras (TLC), designated TLC1, TLC2 and TLC3, were installed along the right bank of the Shár Shaw Tagà River (TLC1 and TLC2: 61°5′26" N, 139°7′34″ W; TLC3: 61°5′12″ N, 139°7′13″ W; Fig. 2). TLC1, installed in 2018, monitored the outwash plain immediately downstream of RG-A1. In 2019, TLC2 was added adjacent to TLC1, extending coverage from the upper margin of TLC1's field of view to the outlet of the N2 subsection of the Shár Shaw Tagà River. Finally, TLC3 was added in 2021 on the bedrock outcrop, oriented toward the N1 subsection, with the upstream outwash plain in the background. All cameras were configured to capture four images daily at 08:00, 11:00, 13:00, and 16:00. Visual analysis of the TLC imagery involved identifying the origins of surface overflow within the riverbed and on the developing aufeis, as well as documenting their occurrence throughout the winter, following the protocol of Chesnokova et al. (2020). Monitoring these overflow events enabled the identification and spatial localization of groundwater outflow points.

3.1.3 Radon activities measurements

Radon (²²²Rn) serves as a natural tracer to detect groundwater exfiltration in streams (Cartwright and Hofmann, 2016). In June 2023, in situ radon activities were measured at two

springs exhibiting the most visible discharge within the N1 subsection: S-RG8, at the RG-A1's front, and S-RG9A, on the opposite talus slope (Fig. 2). Radon activities were also measured in the Shár Shaw Tagà River at the upstream and downstream ends of the N1 subsection (points S-RUP and S-R1, respectively). A portable RAD7 Radon Monitor (Durridge) was used, coupled with the Rad Aqua accessory (Durridge) for radon degassing. Results are reported in Bq m⁻³.

3.2 Physico-hydrochemical characterisation

3.2.1 Sampling and field measurements

Physico-hydrochemical characterisation was undertaken over three campaigns to capture different hydrological conditions: June 2022, August 2022, and June 2023. The June 2022 campaign coincided with the melt of a late and substantial snowpack. The August 2022 campaign took place when glacial ablation was at its peak. The June 2023 campaign was conducted following a winter with reduced snowpack and early snowmelt, after the primary snowmelt phase but before summer glacial ablation commenced, while glaciers remained snow-covered. The three campaigns targeted both the Shár Shaw Tagà River and low-discharge springs along the front of RG-A1 to investigate subsurface connections between the rock glacier and the riverbed (Fig. 2). Additional sites were selected in the proglacial field and in the icedebris complex of the G-B1 subcatchment, hypothesized to be drained by RG-A1 and therefore potentially contributing to the springs. In these areas, all flowing waters were systematically inventoried and sampled. Samples were categorized into four types (Table A1): glacial outlets from the G-B1 snout (S-GL#), streams in the ice-debris complex located between the G-B1 snout and RG-A1 (S-IDC#), springs at the RG-A1 front and opposite talus (S-RG#), and Shár Shaw Tagà River (S-R#). When possible, sites were sampled multiple times within each campaign to account for diurnal fluctuations in physicochemical parameters.

The physico-chemical characterization focuses on natural tracers' analysis for deciphering the origins of the ground-water outflows. Major and minor ions (Ca²⁺, Mg²⁺, Na⁺, Cl⁻, SO₄²⁺, K⁺ and F⁻) were selected for the analysis as their concentrations in water are related to the groundwater residence time and pathways. The natural tracers' analysis includes water stable isotopes too. Field measurements comprehended in situ pH, electrical conductivity (EC, corrected to 25 °C, expressed in μ S cm⁻¹), and water temperature (°C), adding information about groundwater residence time and the presence of frozen content adjacent to groundwater pathways. Measurements for pH, EC and water temperature were taken at each site using a calibrated Hanna HI 98195 multiparameter meter.

Water sampling followed a synoptic approach for cycles of 1–2 d, avoiding precipitation periods (e.g. Baraer et al., 2009). Water samples were filtered using 0.45 µm syringe fil-

ters and collected in 50 mL HDPE bottles, rinsed three times prior to sampling. Not all sites were sampled at each campaign (Table A1), due to various factors (e.g., no flow or safety concerns related to snow cover and rockfalls). Samples for major ion analysis were stored in a dark environment at 4 °C until analysis. Major ions and minor ions were analyzed at the LG2 laboratory, École de technologie supérieure (ÉTS), Montreal, Canada. Cation concentrations were measured using an inductively coupled plasma optical emission spectrometer (5110 ICP-OES, Agilent), and anion concentrations were measured with an ion chromatograph (Dionex ED50, Thermo Fisher Scientific). Bicarbonate (HCO3?) concentrations were calculated from the charge balance equation, and total dissolved solids (TDS) were derived from the sum of ion concentrations. Stable isotopic composition of the water molecule (δ^{18} O and δ^{2} H) was measured using a cavity ringdown spectrometer (Picarro L2130-i) at ÉTS, Montreal, Canada, expressed in % relative to Vienna Standard Mean Ocean Water (VSMOW). Internal reference waters were used for normalization after every three analysis. Results were interpreted following the methodology of Baraer et al. (2015). The absolute values of water temperature and EC measured in situ were considered for tracers while means and ranges were used to assess the diversity in physico-chemical composition among the samples for Principal Component analysis (PCA).

3.2.2 Principal Component Analysis and clustering

Principal Component Analysis (PCA) was used to classify the origins of the sampled water and to identify sample groups that influence the chemistry of the Shár Shaw Tagà River. For each of the three sampling campaigns, PCA was performed using a set of independent variables: water temperature, δ^{18} O, Na⁺, Mg²⁺, Ca²⁺, and SO₄²⁺. These major ions were selected as they exhibited concentrations above the detection limit in more than 95 % of the samples. Principal components explaining at least 90 % of the total variance were retained for further analysis to ensure the robustness of the PCA.

After conducting PCA, clustering analysis was performed using the *k*-means algorithm for each campaign (Lloyd, 1982; MacQueen, 1967). This analysis was based on the sample scores derived from the selected principal components. The maximum number of clusters was set at 25 % of the total number of samples for each campaign, which corresponded to 5, 9 and 7 for the campaigns of June 2022, August 2022, and June 2023, respectively. The algorithm determined the resulting clusters were by associating samples with dominant combinations of variables, thereby highlighting inherent patterns within the dataset.

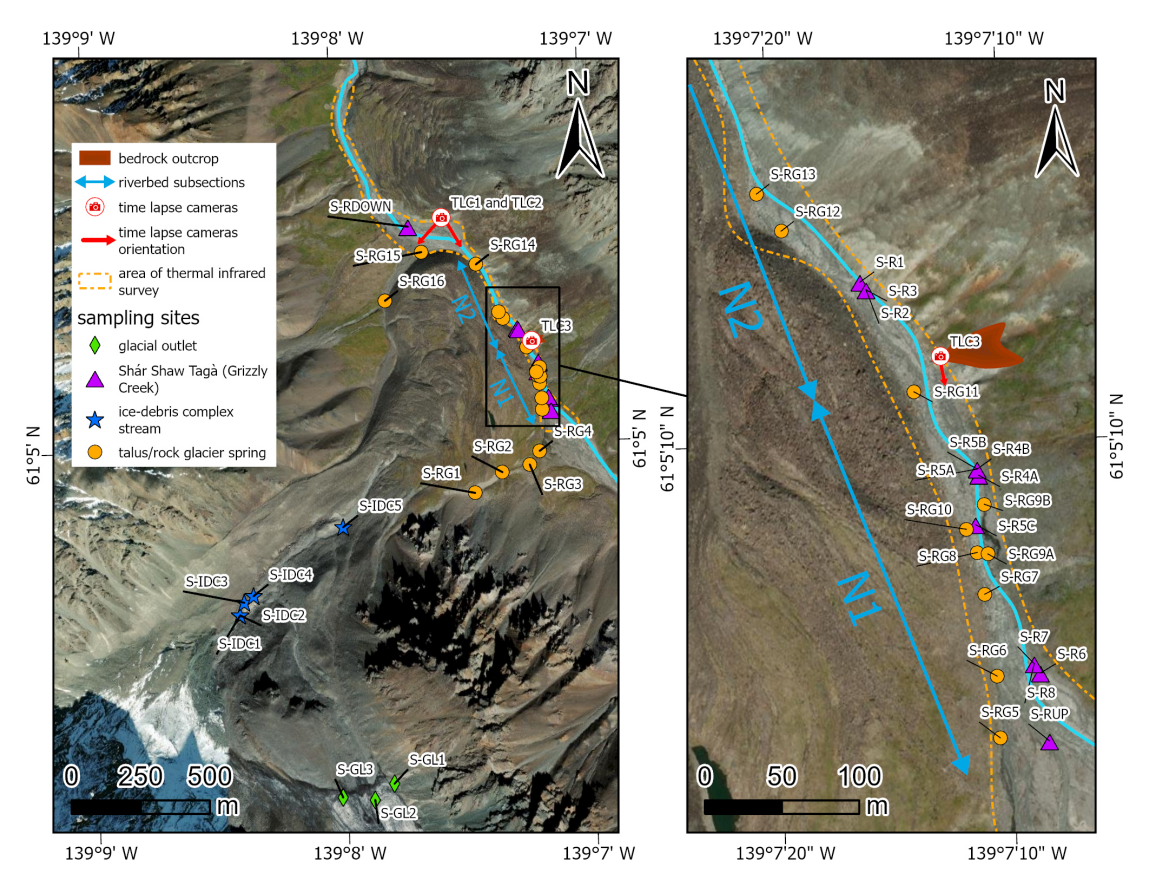


Figure 2. Extent of the TIR survey and locations of sampling sites and TLC cameras. Panel (a) corresponds to the study area, while panel (b) provides a zoom-in of panel (a). A bedrock outcrop on the talus slope opposite to RG-A1 marks the division of the Shár Shaw Tagà River's "narrow section" into two subsections, N1 and N2, as shown on the map. The spring locations represent the outflow points observed during the August 2022 campaign, though their positions may vary depending on hydro-meteorological conditions. Basemap credits: Esri.

4 Results

4.1 Monitoring and surveying of groundwater exfiltration

4.1.1 TIR survey

The TIR survey identified cold-water emergence zones in the downstream outwash plain and within the N1 subsection of the Shár Shaw Tagà River's "narrow section". Emergence zones from the left bank were labeled TIR-L#, and those from the right bank were labeled TIR-R#. In the imagery, these zones appeared as distinct color contrasts separating warmer surface waters from colder emergences (Fig. 3a). At each site, the mixing plumes were mapped. In the most prominent emergence zones (plumes > 2 m in length), the visible video footage also showed clearer water, which provided additional confirmation of groundwater emergence (Fig. 3b).

The TIR survey detected four cold emergence zones in the outwash plain downstream of RG-A1 (Fig. 4). Two cold emergence zones were identified on the left bank: one was observed to be associated with meltwater originating from a snow patch at the front of RG-A1, and the other was observed to be from a persistent snow patch on the west flank of the valley. The other two cold emergence zones were located on the right bank, originating from the middle of the outwash plain near the front of RG-B2. These four cold emergence zones are considered not fed by RG-A1, as they originate from snow patches or from the right bank and could not be related to any sampled spring.

Within the "narrow section", eight cold-water emergence zones were identified in the N1 subsection on the left bank of the main channel, and six on the right bank (Fig. 4). No cold-water emergence zone was detected in the N2 subsection. The furthest downstream cold emergence zone in the N1 subsection (TIR-L8) is located just a few meters upstream of the bedrock outcrop. Cold emergence zones on the left bank are generally smaller, with plume lengths ranging from 1 to 6 m, four of these less than 2 m long. In contrast, cold emergence zones on the right bank are larger, with plume lengths ranging from 5 to 14 m, and four exceed 10 m in length.

Of the six cold emergence zones identified on the right bank of the N1 subsection, two were located within a few

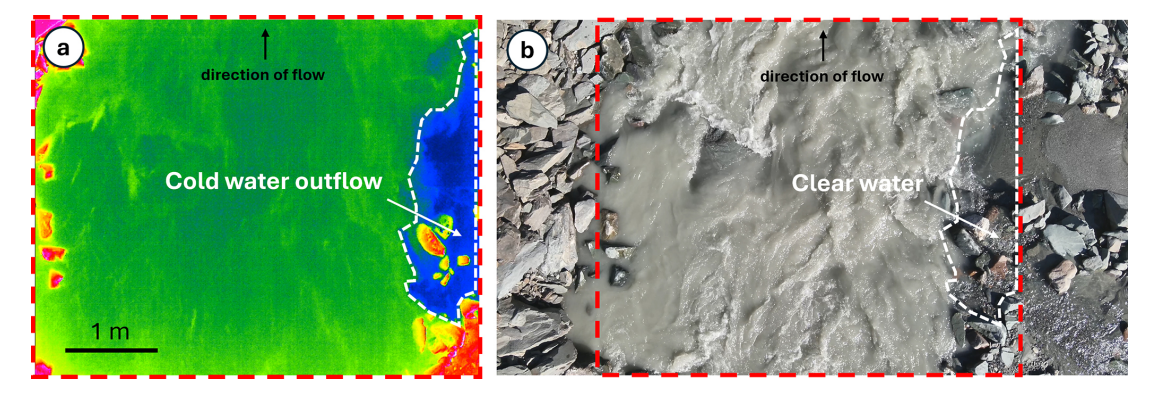


Figure 3. (a) TIR capture showing cold groundwater emergence (in blue, delimited by the dashed white line), mixing with the warmer waters of the Shár Shaw Tagà River (in green) at the TIR-R2 location. Note that the video does not provide a color scale. (b) RGB image capture showing clear water flowing into the Shár Shaw Tagà River, which is characterized by a significant sediment load at the TIR-R2 location. The cold emergence zone detected with TIR is delimited by the dashed white line. The extent of the TIR capture is indicated by the dashed red line. Flight data and information can be accessed as supplemental material in Charonnat and Baraer (2025).

meters of springs sampled in 2022 and 2023 (TIR-R2 and TIR-R3 can be associated to S-RG9A and S-RG9B, respectively). On the left bank, no cold emergence zone was detected in 2024 directly at the position of springs sampled in 2022 and 2023. However, as noted in Sect. 2, the outflow positions of springs on the left side of the river can shift 10–20 m downstream of the RG-A1 front, depending on river level and meteorological conditions. During the 2024 TIR survey, such conditions prevailed, and cold emergence zones were detected 20 m downstream of springs sampled in 2022 and 2023. Accordingly, cold emergence zones TIR-L1, TIR-L2, and TIR-L8 can be linked to springs S-RG8, S-RG10, and S-RG11, respectively (Fig. 4).

Overall, the drone-based TIR survey revealed a high density of cold water emergence zones along both the left and right banks of the N1 subsection, upstream of the bedrock outcrop. These zones, connected to springs sampled in 2022 and 2023, delineate a significant area of groundwater exfiltration within the upstream half of the "narrow section" of the Shár Shaw Tagà River, where flow is constrained by RG-A1 rock glacier.

4.1.2 TLC monitoring

Over the 2018–2021 period, TLC1 monitored aufeis formation during the winters of 2018–2019 and 2019–2020 (Fig. 5). No aufeis formation was observed during the winter of 2020–2021. The onset of aufeis development varied between the two winters. In 2018–2019, it began in early November and continued to develop throughout the winter season, whereas in 2019–2020, it started in February and progressed through February and March (Fig. 5). The development of the aufeis in both winters occurred in phases characterized by multiple flood events. Visible ablation of the aufeis began in May, with complete melt occurring by June in both 2019 and 2020. The aufeis that formed during the winters of

2018–2019 and 2019–2020 spanned the entire width of the river, from the RG-A1 front to the RG-B2 front.

TLC2, installed in 2019 next to TLC1 and oriented towards the aufeis upstream section, recorded the formation of the aufeis in the winter of 2019–2020 and its absence during 2020–2021. In the winter of 2020, TLC2 captured reflections of liquid water and/or ice at the end of the N2 subsection (Fig. 6a and b). In subsequent days, the aufeis was observed to form in the downstream outwash plain, starting from the end of the N2 subsection too.

TLC3, installed in 2021 to monitor surface outflow in the N1 subsection, showed reflections of liquid water and/or ice from the entrance of the N1 subsection (Fig. 6c), while the upstream outwash plain remained without any visible surface outflow. These observations indicate that the liquid water available in winter to supply the aufeis could originate from the "narrow section" between the upstream and the downstream outwash plains. The only winter during which TLC3 was installed to monitor surface flow in the "narrow section" coincided with the sole winter in which no aufeis developed in the downstream outwash plain. This observation suggests that surface flow in this section may play a more significant role in other years.

The monitoring of the aufeis provides evidence of overflow events during late fall and winter, particularly in the 2018–2019 and 2019–2020 periods. The continuous development of aufeis throughout winter, along with its large spatial extent, indicates the presence of a significant and stable water source. The formation of the aufeis is attributed to groundwater outflow from the "narrow section" of the Shár Shaw Tagà River, as the river runs dry in winter and surface outflow is visible from the N1 subsection. This finding aligns with the high density of springs inventoried along the N1 subsection with the TIR imagery.

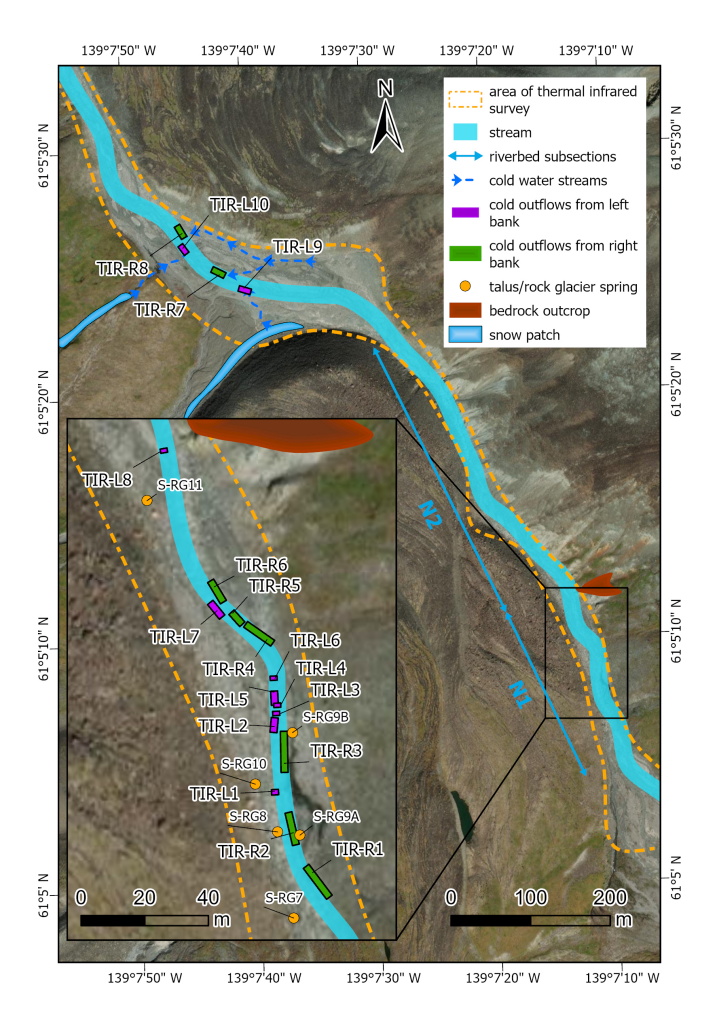


Figure 4. Location of cold-water outflows detected by the TIR survey along the Shár Shaw Tagà riverbed. The zoomed-in view of the "narrow section" highlights an area with a high density of cold groundwater outflows detected on both sides of the river, upstream of a bedrock outcrop constraining the riverbed. Basemap credits: Esri.

4.1.3 Radon activities measurements

In June 2023, while the Shár Shaw Tagà River level was lower than in previous years for the same period, ^{222}Rn activities were similar at S-RG8 and S-RG9A, ranging from $10.17\times 10^3\pm 0.22\times 10^3$ to $10.85\times 10^3\pm 0.19\times 10^3\,\text{Bq}\,\text{m}^{-3}$ (Fig. 7). These springs are located along the N1 subsection of the river, at the left and the right of the stream, respectively. In contrast, the Shár Shaw Tagà River at the upstream end of the N1 subsection (S-RUP) exhibited low activities $(0.36\times 10^3\pm 0.06\times 10^3\,\text{Bq}\,\text{m}^{-3})$, while the downstream end of N1 (S-R1) showed significantly higher activities $(5.46\times 10^3\pm 0.14\times 10^3\,\text{Bq}\,\text{m}^{-3})$. These results clearly indicate groundwater input to the Shár Shaw Tagà River in the N1 subsection, where S-RG8 and S-RG9A are located.

4.2 Physico-hydrochemical characterization

4.2.1 Sampling and field measurements

The mean water temperature of springs at the front of RG-A1 was 0.90 °C in June 2022, slightly colder than in August 2022 and June 2023, respectively exhibiting mean temperatures of 1.38 and 1.40 °C (Table S1 in the Supplement). The colder conditions in June 2022 likely reflect recent snowmelt, whereas no snow cover remained at lower elevations during August 2022 and June 2023. Groundwater outflows with temperatures below 2 °C in late season are commonly interpreted as evidence of adjacent frozen material (Carturan et al., 2024; Haeberli, 1975; Scapozza, 2009). Accordingly, the cold temperatures measured in August 2022 in the springs at the RG-A1's front inform on persistence of frozen content nearthe front of the rock glacier.

High EC ranges (respectively 439.10 and 546.72 μS cm⁻¹ in June and August 2022) underscore the heterogeneous behaviour of the sampled springs. This apparent diversity in physico-chemical composition provides the basis for applying PCA to cluster springs according to their properties.

4.2.2 Principal Component Analysis and clustering

Samples collected in June 2022

Principal Component (PC) 1 accounts for 60.96% of the variance in the dataset and primarily reflects the influence of ionic elements, with PC scores ranging from 0.47 to 0.50 (Fig. 8a). PC2 and PC3, explaining 18.29% and 14.10% of the variance, respectively, exhibit contrasting associations with the $\delta^{18}O$ ratio and temperature. PC2 displays a strong positive correlation with temperature (0.73) and a negative correlation with temperature (-0.67), whereas PC3 shows positive correlations with $\delta^{18}O$ (0.62) and temperature (0.71).

Clustering analysis based on PCA reveals two distinct clusters among the June 2022 samples (Fig. 8b). Cluster 1 comprises 17 samples characterized by low concentrations of mineral elements (Fig. 8c), with total dissolved solids (TDS) concentrations ranging from 28 to $100 \,\mathrm{mg}\,\mathrm{L}^{-1}$. In contrast, Cluster 2 includes samples S-RG4, S-RG5, and S-RG8, which show elevated TDS values (90 to $269 \,\mathrm{mg}\,\mathrm{L}^{-1}$). S-RG5 is grouped within Cluster 2 primarily due to its elevated water temperature, while its other physico-chemical characteristics closely resemble those of the Cluster 1 samples. With the exception of S-RUP, S-RG4, and S-RG15, which record warmer temperatures from 1.43 to 3.19 °C, the remaining 16 samples in the June 2022 dataset exhibit colder temperatures, ranging from 0.03 to 0.67 °C (Fig. 8c). The most enriched samples are S-IDC2, S-RG7, S-RG8, and S-RG10, with δ^{18} O values between -23% and -22.6% vs. VSMOW in δ^{18} O (Fig. 8d).

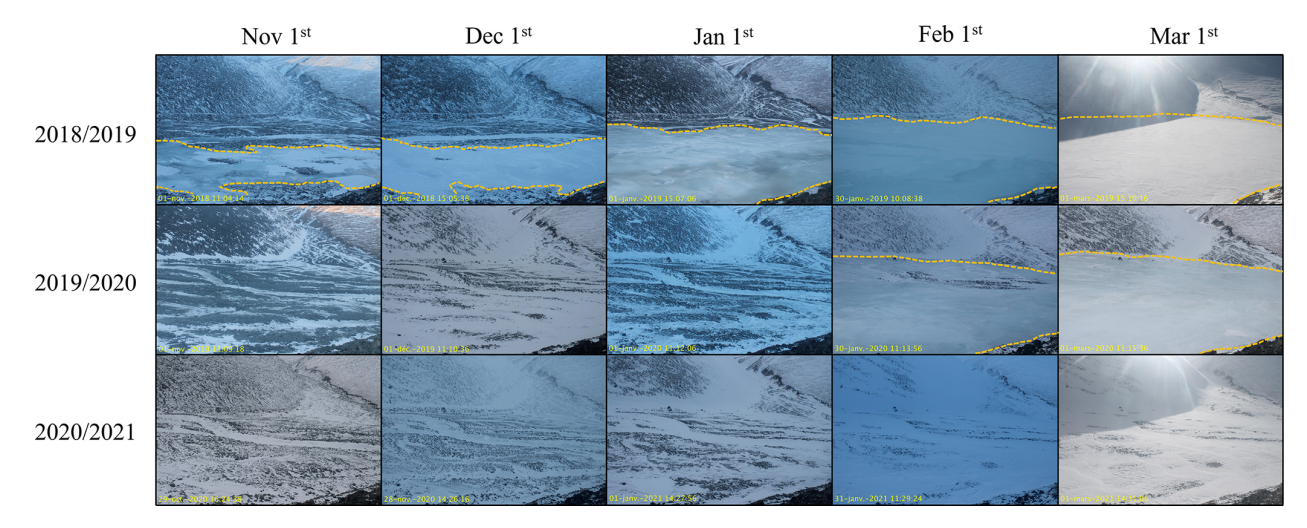


Figure 5. Monthly time-lapse images captured by TLC1 of the aufeis from 1 November to 1 March during the winters of 2018–2019, 2019–2020, and 2020–2021. The yellow dashed line indicates the extent of the aufeis in each image when visible. The time-lapse images were selected targeting the closest to the first day of each month, with consideration given to image quality. Note that no aufeis formation occurred during the 2020–2021 winter.



Figure 6. Winter outflows in the downstream outwash plain (**a**, **b**) and in the N1 subsection (**c**), captured by TLC2 on (**a**) 4 January 2020 at 08:00, (b) 8 January 2020 at 11:00, and TLC3 on (**c**) 22 October 2021 at 13:00. The light in the raw images has been enhanced to improve picture quality. (**a**) and (**b**) are oriented towards the end of the N2 subsection and the entrance of the downstream outwash plain, while (**c**) is oriented towards the N1 subsection and the upstream outwash plain in the background. (**a**) At 08:00 on 4 January 2020, the aufeis has not yet formed, but reflections of ice and/or liquid water are visible at the end of the N2 subsection, during a time when the Shár Shaw Tagà River is dry. (**b**) At 11:00 on 8 January 2020, the aufeis has started to form in the outwash plain, extending from the end of the N2 subsection. (**c**) At 13:00 on 22 October 2021, surface outflow is visible from the entrance of the N1 subsection, but no outflow is visible in the upstream outwash plain in the background.

In June 2022, 17 springs (Cluster 1) were supplied by recent snowmelt, as indicated by low concentrations of mineral elements and cold temperatures. In contrast, S-RG8 and S-RG4 (Cluster 2) were supplied by groundwater, as evidenced by their higher concentrations of mineral elements. The comparatively enriched δ^{18} O values of S-IDC2, S-RG7, S-RG8, and S-RG10 may indicate mixing with a source other than snowmelt, such as glacial meltwater, as they approach the δ^{18} O values measured in glacial meltwater samples collected in August 2022 (see following paragraph).

Samples collected in August 2022

PC1 accounts for 60.57 % of the variance in the dataset and is strongly influenced by solute concentrations, with PC scores

ranging from 0.47 to 0.48 (Fig. 9a). PC2, which explains 22.34 % of the variance, reflects opposing influences of temperature (0.68) and isotopic composition (-0.63). PC3, accounting for 9.01 % of the variance, shows joint positive correlations with both temperature (0.71) and isotopic composition (0.63).

Clustering analysis clearly distinguishes different sample types, forming 9 clusters, the maximum achievable based on the parametrization (Fig. 9b). Cluster 3 consists of glacial outlet samples, characterized by low solute concentrations (16 to $38 \, \mathrm{mg} \, \mathrm{L}^{-1}$ in TDS), cold temperatures (0.06 to 0.07 °C), and depleted isotopic compositions (–21.6 to –22‰ vs. VSMOW in δ^{18} O) as seen in Fig. 9c and d. Clusters 5 and 6 comprise Shár Shaw Tagà River samples, with

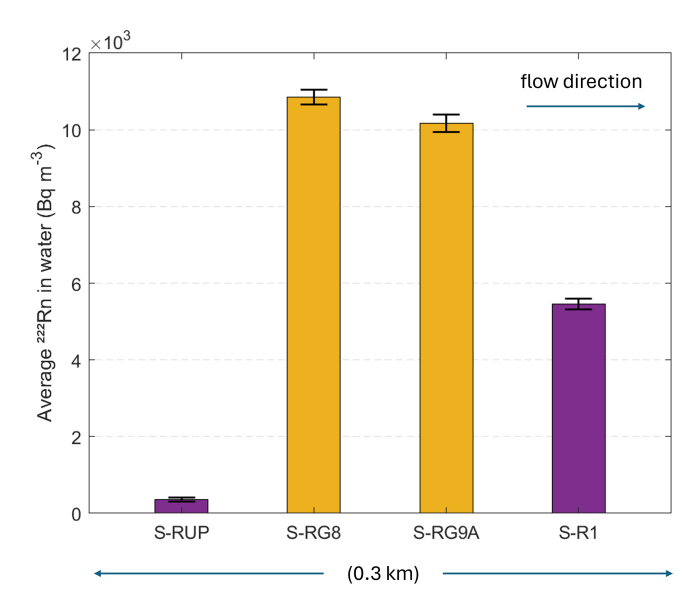


Figure 7. ²²²Rn activities measured with a portable RAD7 Radon Monitor (Durridge) in June 2023. Data were collected at springs S-RG8 and S-RG9A (orange) and along the Shár Shaw Tagà river at upstream (S-RUP) and downstream (S-R1) sites (purple). The bars are arranged from left to right in spatial sequence from upstream to downstream. The error bars represent the uncertainties in the radon activity measurements.

warmer temperatures (3.47 to 6.26 °C), higher solute concentrations (88 to $238 \,\mathrm{mg} \,\mathrm{L}^{-1}$ in TDS), and depleted isotopic compositions (-21.8% to -22.2% vs. VSMOW in δ^{18} O). The distinction between these clusters may be attributed to variations in the glacial regime diurnal cycle and weather conditions based on sampling times. Clusters 4 and 8 include samples from springs near the upper end of the rock glacier front and at the transition area with the icedebris complex (e.g., S-IDC5, S-RG1, S-RG2). As shown in Fig. 9c and d, these springs display high concentrations of mineral elements (209 to 304 mg L^{-1} in TDS) and enriched isotopic compositions (-20.6% to -20.9% vs. VSMOW in δ^{18} O). Clusters 2 and 9 are represented by springs S-RG7, S-RG8, S-RG9A, and S-IDC1, which exhibit high but narrow ranges of solute concentrations (282 to $309 \,\mathrm{mg}\,\mathrm{L}^{-1}$ in TDS) and more depleted isotopic compositions (-21.6% to -21.8% vs. VSMOW in δ^{18} O), as shown in Fig. 9d. Clusters 1 and 7 include other springs from the N1 subsection of the Shár Shaw Tagà River, which are characterized by low solute concentrations (111 to $162 \,\mathrm{mg}\,\mathrm{L}^{-1}$ in TDS) and enriched isotopic compositions (-20.4% to -20.9%vs. VSMOW in δ^{18} O). Figure 9d clearly distinguishes samples with depleted isotopic compositions (below -21.5%vs. VSMOW in $\delta^{18}O$) from those with enriched compositions (above -20.9% vs. VSMOW in δ^{18} O).

In late summer, the hydrochemical signatures of the springs show significant contrasts, with a high number of clusters. However, springs S-RG7, S-RG8, and S-RG9A

share isotopic signatures similar to glacial meltwater from S-G1, S-G2, S-G3, and Shár Shaw Tagà River samples, indicating a glacial input. Despite being located on opposite sides of the river, these springs cluster together, contrasting with the other springs. 25 rock glacier spring samples show cold temperatures (< 2 °C; Fig. 9c). Other springs appear to originate from summer precipitation, as indicated by their enriched isotopic signatures. Among these, some exhibit short residence times, reflected by low solute concentrations (S-RG5, S-RG6, S-RG12, S-RG13, and S-RG14), whereas others show longer residence times, reflected by higher solute concentrations (S-RG1, S-RG2, and S-IDC5).

Samples collected in June 2023

PCA conducted on samples collected in June 2023 revealed that PC1 accounts for 68.79 % of the variance (Fig. 10a), primarily driven by solute concentrations (PC scores ranging from 0.40 to 0.48). PC2 and PC3 explain 15.54 % and 10.43 % of the variance, respectively. PC2 is mainly influenced by water temperature (0.88), while PC3 is dominated by isotopic composition (0.86).

The glacier outlet samples form a distinct cluster, labeled as Cluster 3 (Fig. 10b). The remaining samples are divided into two clusters, with a clear distinction based on the maximum number of clusters (5). Cluster 1 consists solely of Shár Shaw Tagà River samples from the upstream part of the N1 subsection. Cluster 2 includes spring samples and Shár Shaw Tagà River samples collected in the downstream part of the N1 subsection. River samples from the downstream N1 subsection and spring samples exhibit higher solute concentrations (from 121 to 147 mg L^{-1} in TDS) and colder temperatures (from 0.7 to 4° C, with 14 out of 16 samples $< 2^{\circ}$ C) compared to the upstream N1 samples, which have lower solute concentrations (87 to 125 mg L^{-1}) and warmer temperatures (5.3 to 9.5 °C; Fig. 10c). The isotopic composition is generally more enriched for the upstream N1 river samples than for the downstream N1 river and spring samples (Fig. 10d). The isotopic composition of one of the two glacial water samples from G-B1 (sample S-GL1) is similar to the composition from the Shár Shaw Tagà River in upstream N1 (water flowing from G-A1). However, the second S-GL1 sample shows a much more enriched isotopic composition, due to a two-day interval between the respective samplings. The most enriched sample (-21.2% vs. VSMOW in δ^{18} O and -165.4% vs. VSMOW in δ^2 H) was taken first, when the G-B1 glacier was still snow-covered. The most depleted sample (-22.4% vs. VSMOW in δ^{18} O and -173.6% vs. VSMOW in δ^2 H) was taken two days later, following significant snowmelt cover on G-B1 and the initiation of glacial

The springs located on opposite sides of the river along the N1 subsection cluster together (Cluster 2) and exhibit close hydrochemical signatures, similar to what was observed in August 2022. By distinguishing between two clusters, the

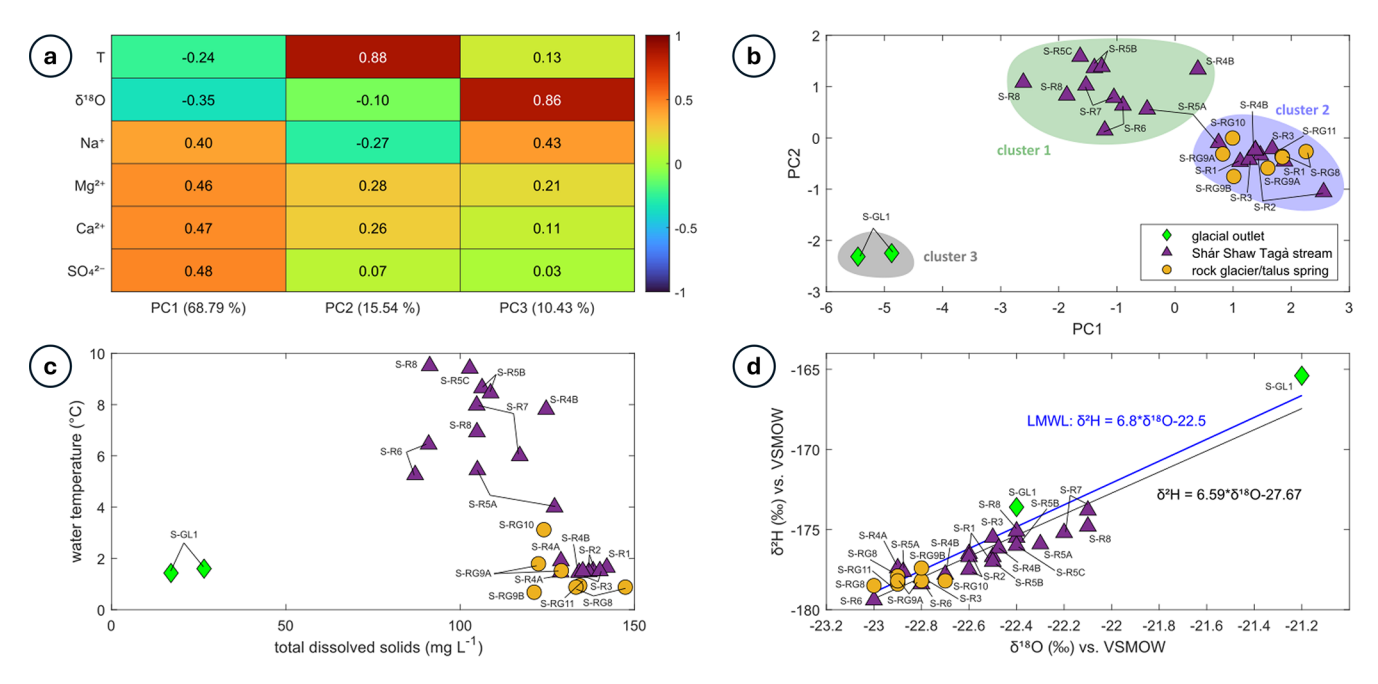


Figure 8. (a) PCA scores for June 2022 samples. The explained variance for each PC is indicated in the legend of the horizontal axis. (b) Distribution of clusters formed from June 2022 samples following PCA and *k*-means clustering. Symbols represent different sample types, and ellipses illustrate the distribution of each cluster. (c) Distribution of total dissolved solids (TDS) concentrations and water temperature for the June 2022 samples. (d) Isotopic composition of the June 2022 samples.

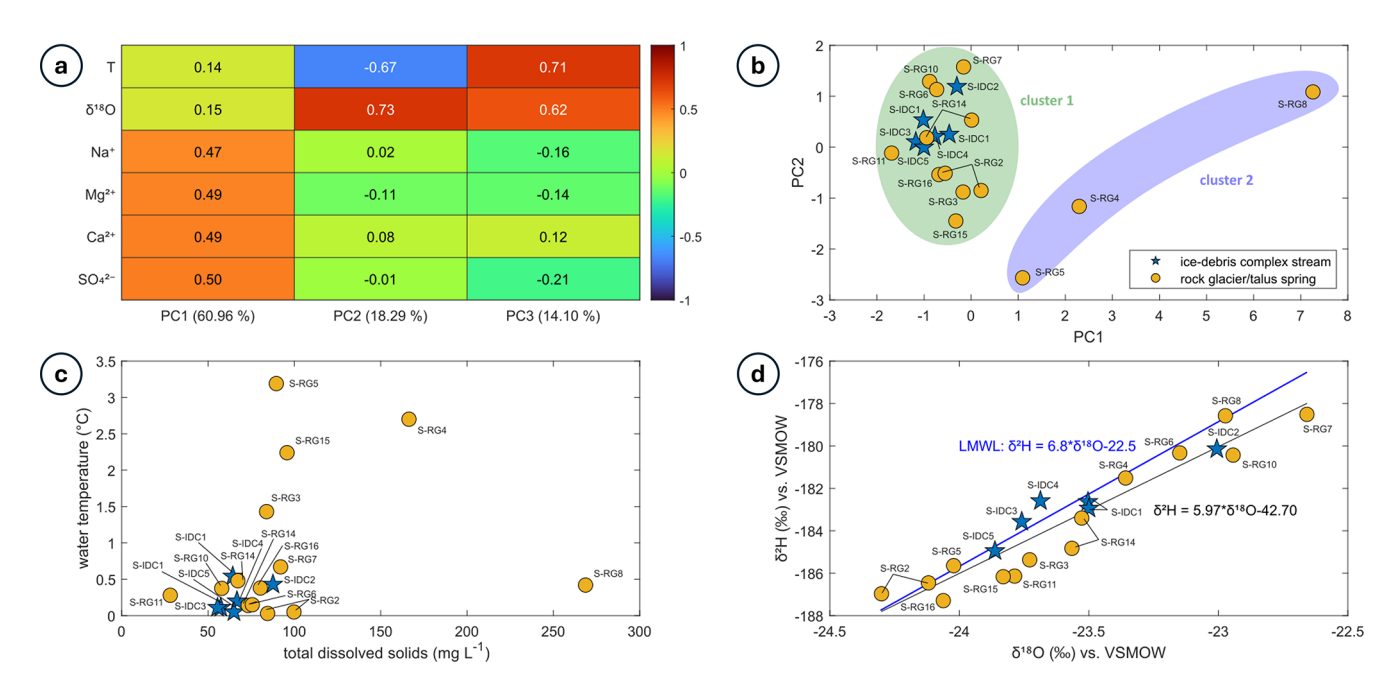


Figure 9. (a) PCA scores for August 2022 samples. The explained variance for each PC is indicated in the legend of the horizontal axis. (b) Distribution of clusters formed from August 2022 samples following PCA and *k*-means clustering. Symbols represent different sample types, and ellipses illustrate the distribution of each cluster. (c) Distribution of total dissolved solids (TDS) concentrations and water temperature for the August 2022 samples. (d) Isotopic composition of the August 2022 samples.

PCA highlights the important influence of these springs on the Shár Shaw Tagà River. Their outflows significantly lower the water temperature and increase solute concentrations in the river.

Synthesis of physico-hydrochemical characterisation

The springs surrounding RG-A1's front exhibit heterogeneous hydrochemical signatures, highlighting their connection to different drainage systems. A group of springs along the N1 subsection (S-RG7, S-RG8, and S-RG9A) cluster together in PCA and share high EC values, depleted isotopic compositions, high solute concentrations. Despite being located on opposite sides of the river, these three springs show striking similarities, suggesting a common origin. Their isotopic compositions are comparable to those of glacial meltwater sampled at the snout of G-B1 and in the Shár Shaw Tagà River, differing significantly from other springs along RG-A1's front. The other springs at the RG-A1's front exhibit diverse hydrochemical signatures under varying hydrometeorological conditions. However, they exhibit signatures of recent precipitation, originating from snowmelt in the early season or rainfall in the late season. Variations in solute concentrations reveal both short and prolonged residence times among these springs, indicating distinct groundwater flow pathways. Most of the springs consistently exhibit cold temperatures, suggesting flow path adjacent to frozen content. During low-discharge periods, such as June 2023, the springs along the N1 subsection considerably increase downstream solute concentrations and radon activities in the Shár Shaw Tagà River, while their cold outflows reduce stream temperature.

5 Discussion

5.1 Indirect influence of the rock glacier

The TIR survey, aufeis monitoring and radon activities measurements identified a major zone of groundwater emergence in the N1 subsection of the Shár Shaw Tagà River, connected to springs both at the front of the rock glacier and on the opposite talus slope. TLC monitoring confirmed that this zone remains active during winter. Physico-hydrochemical characterization indicates that springs on both banks of the N1 subsection share a glacial meltwater signature. No evidence was found for outflow originating from the head of the rock glacier's subcatchment (fed by glaciers G-B1 and G-B2). Furthermore, contributions from internal ice melt to rock glacier discharge are minimal and exert little influence on isotopic concentrations (Croce and Milana, 2002; Krainer and Mostler, 2002; Krainer et al., 2007).

Thus, these springs do not represent outlets of the rock glacier's internal drainage system. Instead, their similar physico-hydrochemical composition indicate the emerging water originates from the same glacial source, which is coherent with field observations. Located on opposite banks of the river, these springs are fed exclusively by upstream outwash plains of the main Shár Shaw Tagà catchment. In June 2023, surface flow temporarily ceased upstream of the outwash plain, resuming only in the N1 subsection via groundwater inflows. Together, these observations indicate that springs in the N1 subsection are not sourced from the rock glacier, but are rather sustained by a shallow aquifer recharged by upstream glacial meltwater, potentially infiltrating the riverbed or the glacier bed.

Parafluvial flow is common in outwash plains with coarse-grained unconsolidated sediments, occurring in river reaches where water is lost before rejoining the river in gaining reaches (Cartwright and Hofmann, 2016). Such plains, often underlain by bedrock, retain groundwater in the shallow subsurface and provide baseflow during low-discharge periods (Müller et al., 2024). In this case, the parafluvial and shallow groundwater resurgence is visible during low-flow periods. The variable location of the springs between sampling campaigns reflects the changes in stored groundwater volume in the alluvial aquifer. The lower density of springs beyond the bedrock outcrop at the downstream end of the N1 subsection suggests a shallow bedrock interface with limited groundwater flow capacity.

Cold temperatures in the springs of the N1 subsection indicate that outflows are cooled by adjacent frozen content, such as massive ice or permafrost (e.g. Carturan et al., 2024). Frozen content has been confirmed within the rock glacier by Evin et al. (1997), and is suspected within the talus slope, based on Scapozza (2015). Frozen material on both banks constrains the alluvial aquifer, forcing groundwater to emerge through springs and cold-water upwellings. The narrowing of the riverbed by the advancing rock glacier further enforces this constraint. Consequently, the resurgences in the N1 subsection can be explained by the rock glacier's geomorphic properties: the combination of riverbed narrowing and obstruction by frozen content constrains subsurface flow, demonstrating an indirect hydrological role through geomorphic control.

This indirect influence produces a high density of cold springs (< 2 °C) along the N1 subsection with distinct physicochemical signatures. The resurgences substantially affect downstream river composition and promote aufeis formation. Solute enrichment in these springs arises from waterrock interactions along groundwater flow paths, with prolonged residence time facilitating the accumulation of dissolved solutes (Hem, 1985). Proximity to buried ground ice and permafrost within the rock glacier and opposite talus slope may further enhance the release of mineral elements through thermal erosion of the ice-sediment matrix (Jones et al., 2019). Physico-hydrochemical characterization from June 2023 demonstrates that, during dry periods, these springs notably increase solute concentrations and radon activities, while simultaneously cooling river water.

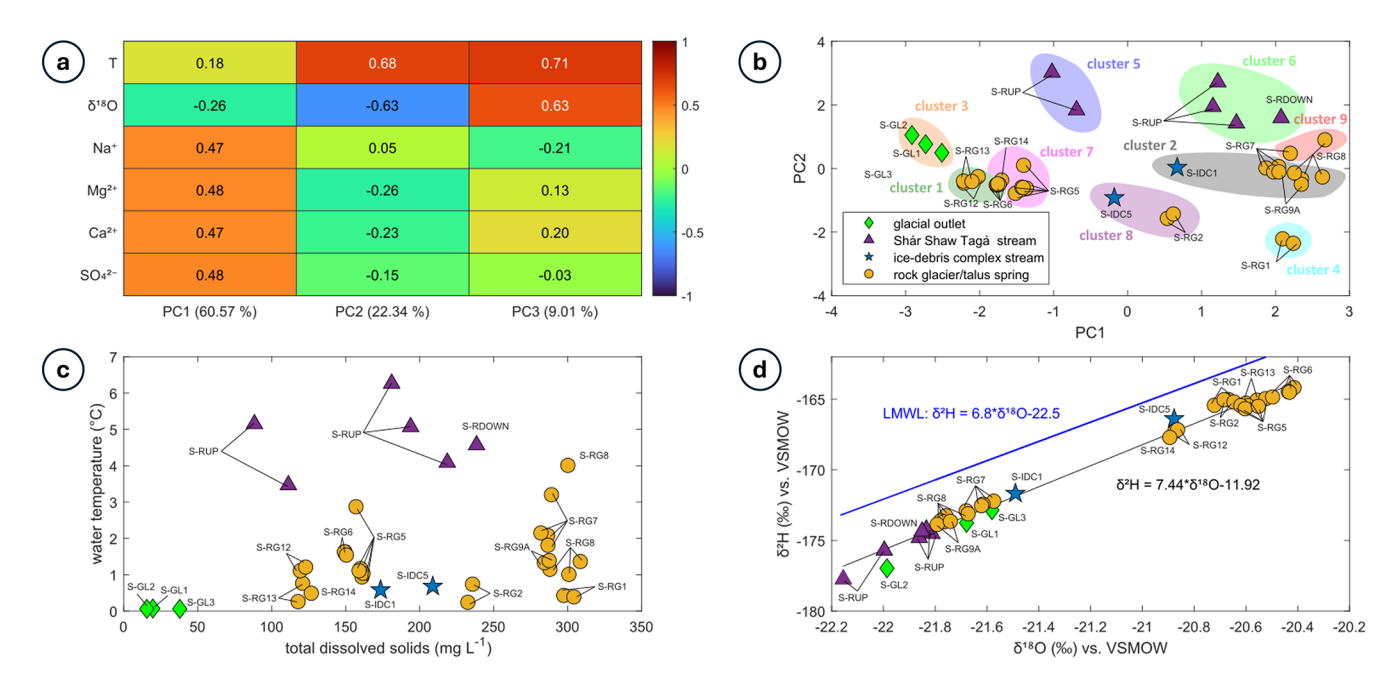


Figure 10. (a) PCA scores for June 2023 samples. The explained variance for each PC is indicated in the legend of the horizontal axis. (b) Distribution of clusters formed from June 2023 following PCA and *k*-means clustering. Symbols represent different sample types, and ellipses illustrate the distribution of each cluster. (c) Distribution of total dissolved solids (TDS) concentrations and water temperature for the June 2023 samples. (d) Isotopic composition of the June 2023 samples.

The consequences of the rock glacier's indirect influence are comparable with the direct impact of rock glaciers outflows on the physicochemical characteristics of downstream surface waters, demonstrated in previous studies (e.g., Bearzot et al., 2023; Brighenti et al., 2023; Robinson et al., 2022; Wagner et al., 2021). Yet, our results indicate that rock glaciers can also exert this influence on riverbed systems primarily in an indirect manner, through their geomorphic and thermal properties – a mechanism not previously documented in the literature.

5.2 Direct influence of the rock glacier

The other springs emerging at the rock glacier front outside the N1 subsection, or within the N1 subsection but not forming a major groundwater emergence area, appear to be associated with the rock glacier's internal drainage system. These springs exhibit limited discharge and exert minimal influence on the riverbed. They are primarily sustained by snowmelt in early season and by summer precipitation later in the season, with little to no contribution from glacial melt, as indicated by the physico-hydrochemical characterization of samples collected in June and August 2022. In Canada, precipitation is typically enriched in heavy isotopes during the snowfree period and depleted during winter and spring (Gibson et al., 2020). Accordingly, the depleted isotopic compositions, low solute concentrations, and cold temperatures measured in early June 2022 point to a snowmelt origin, whereas the enriched isotopic compositions in August reflect a stronger rainfall influence. Thus, they are fed by rapid flow paths and respond to meteorological conditions. Variations in solute concentrations among these springs reflect differences in residence time, thereby indicating distinct flow pathways within the rock glacier. Some springs in the N1 subsection likely represent a mix of precipitation-fed and glacier-fed sources, with physicochemical parameters and clustering reflecting these dual contributions depending on hydro-meteorological conditions and timing.

The behaviour and composition of these springs are consistent with observations from other rock glacier hydrology studies (e.g., Jones et al., 2019). Nevertheless, their influence on streamflow discharge and composition appears limited in the immediate vicinity of the rock glacier. Further work beyond the riverbed survey area would be required to locate outflows from the G-B1 and GB-2 subcatchments which could not be detected. The relatively minor impact of these direct outflows contrasts sharply with the substantial indirect influence exerted by resurgences geomorphically constrained by the rock glacier (Sect. 5.1).

5.3 Possible evolution of the rock glacier influence on catchment hydrology

Predicting the future evolution of the system described in Sect. 5.1 and 5.2 is challenging. Nonetheless, several scenarios can be envisaged across different timescales when considering the role of ground ice in constraining the riverbed and driving groundwater resurgences. Frozen content is likely to

persist in depositional landforms for an extended period, as residual ice has been detected in rock glaciers below the modeled elevation limit in multiple cases (e.g., Carturan et al., 2024; Colucci et al., 2019). Future hydrological conditions in alpine catchments are expected to feature a reduced contribution from glaciers, lower discharge and an increased contribution from groundwater and periglacial features to streamflow (Huss et al., 2017; Jones et al., 2019; Zierl and Bugmann, 2005). These conditions were observed during the June 2023 sampling campaign, which took place after the peak of snowmelt and prior to the peak of glacial ablation, resulting in a substantial influence of groundwater resurgences on the Shár Shaw Tagà River. A similar pattern may occur in the future, with rock glacier-driven groundwater outflows gaining importance in the Shár Shaw Tagà River.

However, ongoing cryosphere degradation under rising air temperatures may render this configuration transitory. Permafrost thaw within the rock glacier and the opposite talus slope will likely reduce geomorphic constraints on the riverbed and diminish obstruction of shallow groundwater flow. The dynamic and transient nature of flow paths across the rock glacier has been previously noted (Johnson, 1978). Furthermore, thermal and mechanical erosion induced by shallow groundwater flow could expand the parafluvial flow zone and create alternative subsurface pathways, reducing the hydrological discontinuity and disruptive effects currently imposed by the rock glacier.

5.4 Limitations and perspectives

The physico-hydrochemical characterization in this study was based on three sampling campaigns conducted under varying hydro-meteorological conditions. These diverse settings posed several challenges for water sampling, including issues with accessibility, safety concerns, periods of no flow, and the need to prioritize specific areas. As a result, some sites could not be revisited during every campaign. Consequently, some sites could not be compared across campaigns, and their characterization can remain incomplete. Moreover, fluctuating weather conditions during a single campaign in proglacial environments likely contributed to variations in physicochemical parameters at some sites. When possible, multiple samples were taken at different times or on different days within the same campaign to minimize biases caused by diurnal and meteorological variations.

This study demonstrates that the indirect hydrological influence of rock glaciers can exceed their direct influence. Future research could build on these findings by investigating the hydrological influences of other rock glaciers extending into valley floors to evaluate the representativeness of this case. Such studies would clarify whether similar patterns occur in different settings. Furthermore, monitoring and modelling of comparable configurations could improve predictions of how these systems may evolve and influence catch-

ment hydrology under ongoing cryosphere degradation. The authors strongly encourage further works in this direction.

6 Conclusions

The objective of this study was to simultaneously evaluate the direct and indirect influences of a rock glacier on the hydrology of an alpine riverbed. We aim to provide new insights into the hydrological processes and their evolution, focusing on both surface flow and shallow groundwater fluxes within the Shár Shaw Tagà subcatchment, Yukon, Canada.

We adopted a multi-method approach combining field observations, drone-based thermal infrared (TIR) surveys, aufeis monitoring and radon activities measurements to identify groundwater emergence zones, alongside physico-hydrochemical analyses of water sources. This methodology enabled us to distinguish contributions originating directly from the rock glacier from those sourced from a shallow aquifer recharged by upstream glacial meltwater.

Our results indicate that the indirect influence of the rock glacier on the riverbed system, through its geomorphic and thermal properties constraining subsurface flow, exerts a greater impact on discharge and water chemistry than direct contributions from the rock glacier. The dynamic landform functions as a structural constraint within the riverbed, forcing groundwater resurgence and substantially affecting downstream physicochemical properties and aufeis formation.

The presence of frozen content in the rock glacier and in the opposite talus slope is central to this indirect influence, modulating constraint on the alluvial aquifer and likely governing the evolution of these flows under ongoing deglaciation and permafrost thaw. Understanding this factor is therefore essential for anticipating changes in alpine hydrological systems under climate warming. Our findings highlight that studies of rock glacier hydrology on catchments should account for indirect effects, which can surpass direct contributions and play a critical role in redistributing both surface and subsurface waters in alpine environments.

Appendix A

Table A1. List and description of sites sampled during the three campaigns between June 2022 and August 2023, with UTM coordinates, elevation, dates and times of sampling. Samples are categorized into four distinct types: glacial outlets from the G-B1 glacier snout (S-GL#), ice-debris complex streams in the proglacial area between the glacier tongue and rock glaciers (S-IDC#), Shár Shaw Tagà River (S-R#), and springs from RG-A1 rock glacier front and opposite talus (S-RG#). Sites were not all sampled for every campaign, due to diverse reasons (access and safety issues, no flow, campaign dedicated to a specific area, etc.). When possible, sites were sampled several times to trace potential fluctuations in their physico-chemical signature. When not sampled, the comment "NV" stands for "not visited." The comment "NF," for "no flow," indicates a site not sampled as it was dry when visited.

Sampling sites	Northing (UTM)	Easting (UTM)	Elevation (m a.s.l.)	Comments	Dates and times of sampling		
					June 2022	August 2022	June 2023
S-R1	6773938	601332	1738	Shár Shaw Tagà river (narrow section)	NV	NV	15/06/23 12:50 16/06/23 13:00
S-R2	6773933	601336	1739	Shár Shaw Tagà river (narrow section)	NV	NV	15/06/23 13:07 16/06/23 13:10
S-R3	6773933	601336	1739	Shár Shaw Tagà river (narrow section)	NV	NV	15/06/23 13:25 16/06/23 13:40
S-R4A	6773813	601409	1741	Shár Shaw Tagà river (narrow section)	NV	NV	15/06/23 13:50
S-R4B	6773817	601408	1746	Shár Shaw Tagà river (narrow section)	NV	NV	15/06/23 14:35 16/06/23 14:20
S-R5A	6773817	601408	1746	Shár Shaw Tagà river (narrow section)	NV	NV	15/06/23 14:40 16/06/23 15:10
S-R5B	6773817	601408	1746	Shár Shaw Tagà river (narrow section)	NV	NV	15/06/23 14:10 16/06/23 15:25
S-R5C	6773781	601407	1747	Shár Shaw Tagà river (narrow section)	NV	NV	16/06/23 14:45
S-R6	6773685	601449	1759	Shár Shaw Tagà river (narrow section)	NV	NV	15/06/23 16:40 16/06/23 15:45
S-R7	6773691	601445	1753	Shár Shaw Tagà river (narrow section)	NV	NV	15/06/23 16:50 16/06/23 16:00
S-R8	6773691	601445	1753	Shár Shaw Tagà river (narrow section)	NV	NV	15/06/23 17:00 16/06/23 16:10
S-RDOWN	6774302	600936	1687	Shár Shaw Tagà river (downstream floodplain)	NV	19/08/22 13:05	NV
S-RUP	6773641	601455	1749	Shár Shaw Tagà river (upstream floodplain)	NV	16/08/22 12:00 16/08/22 16:16 17/08/22 13:12 18/08/22 12:35 19/08/22 13:01	NV
S-GL1	6772289	600889	2083	stream at G-B1 snout	NV	18/08/22 18:36	19/06/23 14:35 21/06/23 12:05
S-GL2	6772230	600819	2109	stream at G-B1 snout	NV	18/08/22 18:06	NV
S-GL3	6772239	600703	2086	stream at G-B1 snout	NV	18/08/22 19:03	NV
S-IDC1	6772896	600330	1886	ice-debris complex stream	16/06/22 15:56 18/06/22 17:50	18/08/22 20:29	NV
S-IDC2	6772897	600330	1886	ice-debris complex stream	18/06/22 17:56	NV	NV

Table A1. Continued.

Sampling sites	Northing (UTM)	Easting (UTM)	Elevation (m a.s.l.)	Comments	Dates and times of sampling		
					June 2022	August 2022	June 2023
S-IDC3	6772943	600345	1891	ice-debris complex stream	16/06/22 15:37	NV	NV
S-IDC4	6772967	600379	1893	ice-debris complex stream	16/06/22 17:04	NV	NV
S-IDC5	6773216	600703	1860	ice-debris complex stream	16/06/22 17:40	18/08/22 20:55	NV
S-RG1	6773340	601180	1797	spring at RG-A1 front	NV	17/08/22 11:58 18/08/22 13:52	NV
S-RG2	6773415	601279	1780	spring at RG-A1 front	12/06/22 16:54 19/06/22 15:08	16/08/22 11:15 17/08/22 12:14	NF
S-RG3	6773442	601378	1770	spring at RG-A1 front	19/06/22 14:48	NF	NF
S-RG4	6773492	601414	1770	spring at RG-A1 front	19/06/22 13:52	NF	NF
S-RG5	6773643	601423	1770	spring at RG-A1 front	19/06/22 13:45	16/08/22 11:30 16/08/22 16:04 17/08/22 12:44 18/08/22 12:47 19/08/22 13:46	NV
S-RG6	6773683	601421	1758	spring at RG-A1 front	19/06/22 13:30	16/08/22 12:40 17/08/22 13:05 18/08/22 12:27 19/08/22 13:24	NV
S-RG7	6773736	601413	1746	spring at RG-A1 front	19/06/22 13:18	16/08/22 13:05 17/08/22 13:58 18/08/22 12:14 19/08/22 13:12	NV
S-RG8	6773763	601408	1744	spring at RG-A1 front	19/06/22 12:50	16/08/22 13:15 17/08/22 14:13 18/08/22 11:11 19/08/22 12:34	15/06/23 14:55 16/06/23 14:35
S-RG9A	6773762	601415	1752	spring flowing from talus opposite to RG-A1 front (right bank)	NV	16/08/22 12:13 17/08/22 13:29	15/06/23 14:55 16/06/23 14:25
S-RG9B	6773931	601335	1734	spring from talus opposite to RG-A1 front (right bank)	NV	NV	16/06/23 14:10
S-RG10	6773778	601401	1749	spring at RG-A1 front	19/06/22 12:43	NV	16/06/23 14:00
S-RG11	6773867	601367	1738	spring at RG-A1 front	19/06/22 12:35	NV	16/06/23 13:30
S-RG12	6773971	601281	1726	spring at RG-A1 front	NV	18/08/22 11:56 19/08/22 12:10	NV
S-RG13	6773995	601265	1726	spring at RG-A1 front	NV	16/08/22 13:47 18/08/22 11:40	NV
S-RG14	6774166	601183	1712	spring at RG-A1 front	15/06/22 15:30 19/06/22 14:25	19/08/22 12:30	NV
S-RG15	6774210	600985	1683	spring at RG-A1 front	19/06/22 15:17	NV	NV
S-RG16	6774034	600854	1740	spring at RG-A1 front	19/06/22 15:42	NV	NV

Data availability. The flight data used for the TIR analysis are available as supplemental material in Charonnat and Baraer (2025), on Borealis dataverse (https://doi.org/10.5683/SP3/O57OMY). Additional data supporting this study are available upon request to the corresponding author.

Video supplement. The videos used for the TIR analysis are available as supplemental material in Charonnat and Baraer (2025), on Borealis dataverse (https://doi.org/10.5683/SP3/O57OMY).

Supplement. The supplement related to this article is available online at https://doi.org/10.5194/hess-29-6479-2025-supplement.

Author contributions. Conceptualization: BC and MB. Data curation: BC. Formal analysis: BC, MB, JMD and CM. Funding acquisition: MB and JMM. Investigation: BC, MB, EV, JMD, KW and ED. Methodology: BC, MB, EV and JMD. Project administration: BC, MB, EV and JMD. Supervision: MB, JMD and JMM. Visualization: BC and KW. Writing – original draft preparation: BC. Writing – review & editing: BC, MB, EV, JMD, CM, KW, ED and JMM. All authors have read and agreed to the published version of the manuscript.

Competing interests. The contact author has declared that none of the authors has any competing interests.

Disclaimer. Publisher's note: Copernicus Publications remains neutral with regard to jurisdictional claims made in the text, published maps, institutional affiliations, or any other geographical representation in this paper. While Copernicus Publications makes every effort to include appropriate place names, the final responsibility lies with the authors. Views expressed in the text are those of the authors and do not necessarily reflect the views of the publisher.

Acknowledgements. We are grateful to the Kluane First Nation and the White River First Nation for the opportunity to conduct research on their territory. We thank the Arctic Institute of North America and the University of Calgary for providing us service and access to their facilities at Kluane Lake Research Station. We thank Parks Canada for their collaboration and for issuing permits that allowed us to conduct research within Kluane National Park and Reserve.

Financial support. This research was supported by the Natural Sciences and Engineering Research Council of Canada, grant numbers RGPIN-2020-05612 and RGPNS-2020-05612, and by Natural Resources Canada – Polar Continental Shelf Program, grant number 62723. Additional funding for the expedition was provided by the Research Centre on the Dynamics of the Earth System (GEOTOP).

Review statement. This paper was edited by Daniel Viviroli and reviewed by two anonymous referees.

References

- Abolt, C., Caldwell, T., Wolaver, B., and Pai, H.: Unmanned aerial vehicle-based monitoring of groundwater inputs to surface waters using an economical thermal infrared camera, Optical Engineering, 57, 1, https://doi.org/10.1117/1.oe.57.5.053113, 2018.
- Antonelli, M., Klaus, J., Smettem, K., Teuling, A. J., and Pfister, L.: Exploring Streamwater Mixing Dynamics via Handheld Thermal Infrared Imagery, Water, 9, 5, https://doi.org/10.3390/w9050358, 2017.
- Arenson, L., Hoelzle, M., and Springman, S.: Borehole Deformation Measurements and Internal Structure of Some Rock Glaciers in Switzerland, Permafrost and Periglacial Processes, 13, 117–135, https://doi.org/10.1002/ppp.414, 2002.
- Arenson, L. U., Harrington, J. S., Koenig, C. E. M., and Wainstein, P. A.: Mountain Permafrost Hydrology A Practical Review Following Studies from the Andes, Geosciences, 12, 2, https://doi.org/10.3390/geosciences12020048, 2022.
- Baraer, M., McKenzie, J. M., Mark, B. G., Bury, J., and Knox, S.: Characterizing contributions of glacier melt and ground-water during the dry season in a poorly gauged catchment of the Cordillera Blanca (Peru), Adv. Geosci., 22, 41–49, https://doi.org/10.5194/adgeo-22-41-2009, 2009.
- Baraer, M., McKenzie, J., Mark, B. G., Gordon, R., Bury, J., Condom, T., Gomez, J., Knox, S., and Fortner, S. K.: Contribution of groundwater to the outflow from ungauged glacierized catchments: A multi-site study in the tropical Cordillera Blanca, Peru, Hydrological Processes, 29, 11, https://doi.org/10.1002/hyp.10386, 2015.
- Barclay, J. R., Briggs, M. A., Moore, E. M., Starn, J. J., Hanson, A. E. H., and Helton, A. M.: Where groundwater seeps: Evaluating modeled groundwater discharge patterns with thermal infrared surveys at the river-network scale, Advances in Water Resources, 160, 104108, https://doi.org/10.1016/j.advwatres.2021.104108, 2022.
- Barsch, D.: Rockglaciers: Indicators for the present and former geoecology in high mountain environments, Springer Series in Physical Environment, 16, ISBN 978-3-540-60742-7, 1996.
- Bearzot, F., Colombo, N., Cremonese, E., di Cella, U. M., Drigo, E., Caschetto, M., Basiricò, S., Crosta, G. B., Frattini, P., Freppaz, M., Pogliotti, P., Salerno, F., Brunier, A., and Rossini, M.: Hydrological, thermal and chemical influence of an intact rock glacier discharge on mountain stream water, Science of The Total Environment, 876, 162777, https://doi.org/10.1016/j.scitotenv.2023.162777, 2023.
- Blöthe, J. H., Rosenwinkel, S., Höser, T., and Korup, O.: Rock-glacier dams in High Asia, Earth Surface Processes and Landforms, 44, 808–824, https://doi.org/10.1002/esp.4532, 2019.
- Bodin, X., Schoeneich, P., Deline, P., Ravanel, L., Magnin, F., Krysiecki, J.-M., and Echelard, T.: Le permafrost de montagne et les processus géomorphologiques associés: Évolutions récentes dans les Alpes françaises, Journal of Alpine Research | Revue de géographie alpine, 103–2, https://doi.org/10.4000/rga.2806, 2015.

- Bolch, T. and Marchenko, S.: Significance of glaciers, rockglaciers and ice-rich permafrost in the Northern Tien Shan as water towers under climate change conditions, IHP/HWRP-Berichte, 8, 8, https://doi.org/10.5167/uzh-137250, 2009.
- Briggs, M. A., Hare, D. K., Boutt, D. F., Davenport, G., and Lane, J. W.: Thermal infrared video details multiscale groundwater discharge to surface water through macropores and peat pipes, Hydrological Processes, 30, 2510–2511, https://doi.org/10.1002/hyp.10722, 2016.
- Brighenti, S., Tolotti, M., Bruno, M. C., Engel, M., Wharton, G., Cerasino, L., Mair, V., and Bertoldi, W.: After the peak water: The increasing influence of rock glaciers on alpine river systems, Hydrological Processes, 33, 2804–2823, https://doi.org/10.1002/hyp.13533, 2019.
- Brighenti, S., Engel, M., Dinale, R., Tirler, W., Voto, G., and Comiti, F.: Isotopic and chemical signatures of high mountain rivers in catchments with contrasting glacier and rock glacier cover, Journal of Hydrology, 623, https://doi.org/10.1016/j.jhydrol.2023.129779, 2023.
- Carrivick, J. L. and Heckmann, T.: Short-term geomorphological evolution of proglacial systems, Geomorphology, 287, 3–28, https://doi.org/10.1016/j.geomorph.2017.01.037, 2017.
- Carturan, L., Zuecco, G., Andreotti, A., Boaga, J., Morino, C., Pavoni, M., Seppi, R., Tolotti, M., Zanoner, T., and Zumiani, M.: Spring-water temperature suggests widespread occurrence of Alpine permafrost in pseudo-relict rock glaciers, The Cryosphere, 18, 5713–5733, https://doi.org/10.5194/tc-18-5713-2024, 2024.
- Cartwright, I. and Hofmann, H.: Using radon to understand parafluvial flows and the changing locations of groundwater inflows in the Avon River, southeast Australia, Hydrol. Earth Syst. Sci., 20, 3581–3600, https://doi.org/10.5194/hess-20-3581-2016, 2016.
- Casas-Mulet, R., Pander, J., Ryu, D., Stewardson, M. J., and Geist, J.: Unmanned Aerial Vehicle (UAV)-Based Thermal Infra-Red (TIR) and Optical Imagery Reveals Multi-Spatial Scale Controls of Cold-Water Areas Over a Groundwater-Dominated Riverscape, Frontiers in Environmental Science, 8, https://doi.org/10.3389/fenvs.2020.00064, 2020.
- Chakravarti, P., Jain, V., and Mishra, V.: The distribution and hydrological significance of intact rock glaciers in the north-west Himalaya, Geografiska Annaler, Series A: Physical Geography, 104, 226–244, https://doi.org/10.1080/04353676.2022.2120262, 2022.
- Charonnat, B. and Baraer, M.: Supplemental Material: Drone-Based Thermal Infrared Imagery for Detection of Cold Groundwater Exfiltration in Shár Shaw Tagà, Yukon, Canada, Borealis V1 [data set and video], https://doi.org/10.5683/SP3/O57OMY, 2025.
- Chesnokova, A., Baraër, M., and Bouchard, É.: Proglacial icings as records of winter hydrological processes, The Cryosphere, 14, 4145–4164, https://doi.org/10.5194/tc-14-4145-2020, 2020.
- Colombo, N., Ferronato, C., Vittori Antisari, L., Marziali, L., Salerno, F., Fratianni, S., D'Amico, M. E., Ribolini, A., Godone, D., Sartini, S., Paro, L., Morra di Cella, U., and Freppaz, M.: A rock-glacier pond system (NW Italian Alps): Soil and sediment properties, geochemistry, and trace-metal bioavailability, Catena, 194, https://doi.org/10.1016/j.catena.2020.104700, 2020.
- Colombo, N., Gruber, S., Martin, M., Malandrino, M., Magnani, A., Godone, D., Freppaz, M., Fratianni, S., and Salerno, F.:

- Rainfall as primary driver of discharge and solute export from rock glaciers: The Col d'Olen Rock Glacier in the NW Italian Alps, Science of the Total Environment, 639, 316–330, https://doi.org/10.1016/j.scitotenv.2018.05.098, 2018.
- Colombo, N., Salerno, F., Martin, M., Malandrino, M., Giardino, M., Serra, E., Godone, D., Said-Pullicino, D., Fratianni, S., Paro, L., Tartari, G., and Freppaz, M.: Influence of permafrost, rock and ice glaciers on chemistry of high-elevation ponds (NW Italian Alps), Science of the Total Environment, 685, 886–901, https://doi.org/10.1016/j.scitotenv.2019.06.233, 2019.
- Colucci, R. R., Forte, E., Žebre, M., Maset, E., Zanettini, C., and Guglielmin, M. Is that a relict rock glacier?, Geomorphology, 330, 177–189, https://doi.org/10.1016/j.geomorph.2019.02.002, 2019.
- Croce, F. and Milana, J.: Internal structure and behavior of a Rock Glacier in the arid Andes of Argentina, Permafrost and Periglacial Processes, 13, 289–299, https://doi.org/10.1002/ppp.431, 2002.
- Delaloye, R., Lambiel, C., and Gärtner-Roer, I.: Overview of rock glacier kinematics research in the Swiss Alps, Geogr. Helv., 65, 135–145, https://doi.org/10.5194/gh-65-135-2010, 2010.
- Dodds, C. J. and Campbell, R. B.: Overview, legend and mineral deposit tabulations for: GSC Open File 2188 to Open File 2191, Geological Survey of Canada, Energy Mines and Resources Canada, 85 p. + 5 maps, https://emrlibrary.gov.yk.ca/gsc/open_files/2191/2191_report/of_2191.pdf (last access: 14 November 2025), 1992.
- Dugdale S. J.: A practitioner's guide to thermal infrared remote sensing of rivers and streams: recent advances, precautions and considerations, WIREs Water, 3, 251–268, https://doi.org/10.1002/wat2.1135, 2016.
- Engel, M., Penna, D., Bertoldi, G., Vignoli, G., Tirler, W., and Comiti, F.: Controls on spatial and temporal variability in streamflow and hydrochemistry in a glacierized catchment, Hydrol. Earth Syst. Sci., 23, 2041–2063, https://doi.org/10.5194/hess-23-2041-2019, 2019.
- Ensom, T., Makarieva, O., Morse, P., Kane, D., Alekseev, V., and Marsh, P.: The distribution and dynamics of aufeis in permafrost regions, Permafrost and Periglacial Processes, 31, 383–395, https://doi.org/10.1002/ppp.2051, 2020.
- Evin, M., Fabre, D., and Johnson, P. G.: Electrical Resistivity Measurements on the Rock Glaciers of Grizzly Creek, St Elias Mountains, Yukon, Permafrost and Periglacial Processes, 8, 11, https://doi.org/10.1002/(SICI)1099-1530, 1997.
- Falatkova, K., Šobr, M., Slavík, M., Bruthans, J., and Janský, B.: Hydrological characterization and connectivity of proglacial lakes to a stream, Adygine ice-debris complex, northern Tien Shan, Hydrological Sciences Journal, 65, 610–623, https://doi.org/10.1080/02626667.2020.1711913, 2020.
- Gibson, J. J., Holmes, T., Stadnyk, T. A., Birks, S. J., Eby, P., and Pietroniro, A.: ¹⁸O and ²H in streamflow across Canada, Journal of Hydrology: Regional Studies, 32, 100754, https://doi.org/10.1016/j.ejrh.2020.100754, 2020.
- Haeberli, W.: Untersuchungen zur Verbreitung von Permafrost zwischen Flüelapass und Piz Grialetsch (Graubünden), Mitteilungen der VAW ETH Zürich, 17, 1–221, 1975.
- Halla, C., Blöthe, J. H., Tapia Baldis, C., Trombotto Liaudat, D., Hilbich, C., Hauck, C., and Schrott, L.: Ice content and interannual water storage changes of an active rock glacier in

- the dry Andes of Argentina, The Cryosphere, 15, 1187–1213, https://doi.org/10.5194/tc-15-1187-2021, 2021.
- Harrington, J. S., Mozil, A., Hayashi, M., and Bentley, L. R.: Groundwater flow and storage processes in an inactive rock glacier, Hydrological Processes, 32, 3070–3088, https://doi.org/10.1002/hyp.13248, 2018.
- Harrison, S., Jones, D., Anderson, K., Shannon, S., and Betts, R. A.: Is ice in the Himalayas more resilient to climate change than we thought? Geografiska Annaler, Series A: Physical Geography, 103, 1–7, https://doi.org/10.1080/04353676.2021.1888202, 2021.
- Hayashi, M.: Alpine Hydrogeology: The Critical Role of Groundwater in Sourcing the Headwaters of the World, Groundwater, 58, 498–510, https://doi.org/10.1111/gwat.12965, 2020.
- Hem, J. D.: Study and Interpretation of the Chemical Characteristics of Natural Water, 3rd Edn., US Geological Survey Water-Supply Paper 2254, University of Virginia, Charlottesville, 263 pp., https://doi.org/10.3133/wsp2254, 1985.
- Hewitt, K. (Ed.): Rock Glaciers and Related Phenomena, in: Glaciers of the Karakoram Himalaya: Glacial Environments, Processes, Hazards and Resources, Springer Netherlands, 267–289 https://doi.org/10.1007/978-94-007-6311-1_11, 2014.
- Hock, R., Rasul, G., Adler, C., Cáceres, B., Gruber, S., Hirabayashi, Y., Jackson, M., Kääb, A., Kang, S., Kutuzov, S., Milner, Al., Molau, U., Morin, S., Orlove, B., and Steltzer, H.: High Mountain Areas, in: IPCC Special Report on the Ocean and Cryosphere in a Changing Climate, edited by: Pörtner, H.-O., Roberts, D. C., Masson-Delmotte, V., Zhai, P., Tignor, M., Poloczanska, E., Mintenbeck, K., Alegriìa, A., Nicolai, M., Okem, A., Petzold, J., Rama, B., and Weyer, N. M., Cambridge University Press, Cambridge, UK and New York, NY, USA, 131–202, https://doi.org/10.1017/9781009157964.004, 2019.
- Huss, M., Bookhagen, B., Huggel, C., Jacobsen, D., Bradley, R. S.,
 Clague, J. J., Vuille, M., Buytaert, W., Cayan, D. R., Greenwood,
 G., Mark, B. g., Milner, A. M., Weingartner, R., and Winder, M.:
 Toward mountains without permanent snow and ice, Earth's Future, 5, 418–435, https://doi.org/10.1002/2016EF000514, 2017.
- Iwasaki, K., Fukushima, K., Nagasaka, Y., Ishiyama, N., Sakai, M., and Nagasaka, A.: Real-Time Monitoring and Postprocessing of Thermal Infrared Video Images for Sampling and Mapping Groundwater Discharge, Water Resources Research, 59, e2022WR033630, https://doi.org/10.1029/2022WR033630, 2023.
- Iwasaki, K., Nagasaka Y., Ishiyama N., and Nagasaka A.: Thermal imaging survey for characterizing bedrock ground-water discharge: comparison between sedimentary and volcanic catchments, Hydrological Research Letters, 18, 79–86, https://doi.org/10.3178/hrl.18.79, 2024.
- Johnson, P. G.: Rock glacier types and their drainage systems, Grizzly Creek, Yukon Territory, Canadian Journal of Earth Sciences, 15, 1496–1507, https://doi.org/10.1139/e78-155, 1978.
- Jones, D. B., Harrison, S., Anderson, K., and Betts, R. A.: Mountain rock glaciers contain globally significant water stores, Scientific Reports, 8, 1, https://doi.org/10.1038/s41598-018-21244-w, 2018.
- Jones, D. B., Harrison, S., Anderson, K., Shannon, S., and Betts, R. A.: Rock glaciers represent hidden water stores in the Himalaya, Science of The Total Environment, 793, 145368, https://doi.org/10.1016/j.scitotenv.2021.145368, 2021.

- Jones, D. B., Harrison, S., Anderson, K., and Whalley, W. B.: Rock glaciers and mountain hydrology: A review, Earth-Science Reviews, 193, 66–90, https://doi.org/10.1016/j.earscirev.2019.04.001, 2019.
- Käser, D. and Hunkeler, D.: Contribution of alluvial groundwater to the outflow of mountainous catchments, Water Resources Research, 52, 680–697, https://doi.org/10.1002/2014WR016730, 2016.
- Krainer, K. and Mostler, W.: Hydrology of Active Rock Glaciers: Examples from the Austrian Alps, Arctic, Antarctic, and Alpine Research, 34, 142–149, https://doi.org/10.1080/15230430.2002.12003478, 2002.
- Krainer, K., Mostler, W., and Spötl, C.: Discharge from active rock glaciers, Austrian Alps: A stable isotope approach, Austrian Journal of Earth Sciences, 100, 102–112, 2007.
- Kummert, M., Bodin, X., Braillard, L., and Delaloye, R.: Pluridecadal evolution of rock glaciers surface velocity and its impact on sediment export rates towards high alpine torrents, Earth Surface Processes and Landforms, 46, 3213–3227, https://doi.org/10.1002/esp.5231, 2021.
- Lloyd, S.: Least squares quantization in PCM, IEEE Transactions on Information Theory, 28, 129–137, https://doi.org/10.1109/TIT.1982.1056489, 1982.
- MacQueen, J.: Some methods for classification and analysis of multivariate observations, in: Proceedings of the fifth Berkeley symposium on mathematical statistics and probability, 1, 281–297, https://www.jstor.org/stable/jj.13083384 (last access: 14 November 2025), 1967.
- Marcer, M., Cicoira, A., Cusicanqui, D., Bodin, X., Echelard, T., Obregon, R., and Schoeneich, P.: Rock glaciers throughout the French Alps accelerated and destabilised since 1990 as air temperatures increased, Communications Earth & Environment, 2, 1–11, https://doi.org/10.1038/s43247-021-00150-6, 2021.
- Marren, P. M. and Toomath, S. C.: Channel pattern of proglacial rivers: Topographic forcing due to glacier retreat, Earth Surface Processes and Landforms, 39, 943–951, https://doi.org/10.1002/esp.3545, 2014.
- Müller, T., Roncoroni, M., Mancini, D., Lane, S. N., and Schaefli, B.: Current and future roles of meltwater–groundwater dynamics in a proglacial Alpine outwash plain, Hydrol. Earth Syst. Sci., 28, 735–759, https://doi.org/10.5194/hess-28-735-2024, 2024.
- Navarro, G., Valois, R., MacDonell, S., de Pasquale, G., and Díaz, J. P.: Internal structure and water routing of an ice-debris landform assemblage using multiple geophysical methods in the semiarid Andes, Frontiers in Earth Science, 11, https://doi.org/10.3389/feart.2023.1102620, 2023.
- PERMOS: Report 2019-16-19 | PERMOS Swiss Permafrost Monitorinig Network, https://www.permos.ch/doi/permos-rep-2019-16-19 (last access: 17 September 2024), 2019.
- Porter, C., Howat, I., Noh, M.-J., Husby, E., Khuvis, S., Danish, E., Tomko, K., Gardiner, J., Negrete, A., Yadav, B., Klassen, J., Kelleher, C., Cloutier, M., Bakker, J., Enos, J., Arnold, G., Bauer, G., and Morin, P.: ArcticDEM Mosaics, Version 4.1, Harvard Dataverse [data set], https://doi.org/10.7910/DVN/3VDC4W, 2023.
- Rautio, A., Kivimäki, A.-L., Korkka-Niemi, K., Nygård, M., Salonen, V.-P., Lahti, K., and Vahtera, H.: Vulnerability of groundwater resources to interaction with river water in a

- boreal catchment, Hydrol. Earth Syst. Sci., 19, 3015–3032, https://doi.org/10.5194/hess-19-3015-2015, 2015.
- Reato, A., Borzi, G., Martínez, O. A., and Carol, E.: Role of rock glaciers and other high-altitude depositional units in the hydrology of the mountain watersheds of the Northern Patagonian Andes, Science of The Total Environment, 824, 153968, https://doi.org/10.1016/j.scitotenv.2022.153968, 2022.
- Robinson, C. T., Jolidon, C., Consoli, G., Bloem, S., and Ebi, C.: Temporal dynamics in the physico-chemistry of a high-alpine stream network in the Swiss National Park, Eco.Mont, 14(2), 11–23, https://doi.org/10.1553/eco.mont-14-2s11, 2022.
- Scapozza, C.: Contributo dei metodi termici alla prospezione del permafrost montano: esempi dal massiccio della Cima di Gana Bianca (Val Blenio, Svizzera), Bollettino della Società Ticinese di Scienze Naturali 97, 55–66, ISSN 079-1254, 2009.
- Scapozza, C.: Investigation on protalus ramparts in the Swiss Alps, Geogr. Helv., 70, 135–139, https://doi.org/10.5194/gh-70-135-2015, 2015.
- Schreder, S., Sommaruga, R., Psenner, R., Chimani, B., Ganekind, M., and Koinig, K. A.: Changes in air temperature, but not in precipitation, determine long-term trends in water chemistry of high mountain lakes of the Alps with and without rock glacier influence, Science of the Total Environment, 905, https://doi.org/10.1016/j.scitotenv.2023.167750, 2023.
- Scotti, R., Crosta, G. B., and Villa, A.: Destabilisation of Creeping Permafrost: The Plator Rock Glacier Case Study (Central Italian Alps), Permafrost and Periglacial Processes, 28, 224–236, https://doi.org/10.1002/ppp.1917, 2017.
- Sorg, A., Kääb, A., Roesch, A., Bigler, C., and Stoffel, M.: Contrasting responses of Central Asian rock glaciers to global warming, Scientific Reports, 5, https://doi.org/10.1038/srep08228, 2015.
- Toran, L.: Groundwater–Surface Water Interaction, in: Encyclopedia of Water, John Wiley & Sons, Ltd, 1–12, https://doi.org/10.1002/9781119300762.wsts0027, 2019.
- Torgersen C. E., Faux R. N., McIntosh B. A., Poage N. J., and Norton D. J.: Airborne thermal remote sensing for water temperature assessment in rivers and streams, Remote Sensing of Environment, 76, 386–398, https://doi.org/10.1016/S0034-4257(01)00186-9, 2001.
- van Tiel, M., Aubry-Wake, C., Somers, L., Andermann, C., Avanzi, F., Baraer, M., Chiogna, G., Daigre, C., Das, S., Drenkhan, F., Farinotti, D., Fyffe, C. L., de Graaf, I., Hanus, S., Immerzeel, W., Koch, F., McKenzie, J. M., Müller, T., Popp, A. L., and Yapiyev, V.: Cryosphere–groundwater connectivity is a missing link in the mountain water cycle, Nature Water, 2, 624–637, https://doi.org/10.1038/s44221-024-00277-8, 2024.
- Vélez-Nicolás, M., García-López, S., Barbero, L., Ruiz-Ortiz, V., and Sánchez-Bellón, Á.: Applications of Unmanned Aerial Systems (UASs) in Hydrology: A Review, Remote Sensing, 13, 7, https://doi.org/10.3390/rs13071359, 2021.

- Wagner, T., Brodacz, A., Krainer, K., and Winkler, G.: Active rock glaciers as shallow groundwater reservoirs, Austrian Alps, Grundwasser, 25, 215–230, https://doi.org/10.1007/s00767-020-00455-x, 2020.
- Wagner, T., Kainz, S., Krainer, K., and Winkler, G.: Storage-discharge characteristics of an active rock glacier catchment in the Innere Ölgrube, Austrian Alps, Hydrological Processes, 35, https://doi.org/10.1002/hyp.14210, 2021.
- Wagner, T., Pauritsch, M., and Winkler, G.: Impact of relict rock glaciers on spring and stream flow of alpine watersheds: Examples of the Niedere Tauern Range, Eastern Alps (Austria), Austrian Journal of Earth Sciences, 109, https://doi.org/10.17738/ajes.2016.0006, 2016.
- Wahl, H. E., Fraser, D. B., Harvey, R. C., and Maxwell, J. B.: Climate of Yukon, Atmospheric Environment Service, Environment Canada, ISBN 0660124157, 1987.
- Wanner, C., Moradi, H., Ingold, P., Cardenas Bocanegra, M. A., Mercurio, R., and Furrer, G.: Rock glaciers in the Central Eastern Alps How permafrost degradation can cause acid rock drainage, mobilization of toxic elements and formation of basaluminite, Global and Planetary Change, 227, https://doi.org/10.1016/j.gloplacha.2023.104180, 2023.
- Webb, B. W., Hannah, D. M., Moore, R. D., Brown, L. E., and Nobilis, F.: Recent advances in stream and river temperature research, Hydrological Processes, 22, 902–918, https://doi.org/10.1002/hyp.6994, 2008.
- Winkler, G., Wagner, T., Pauritsch, M., and Kellerer-Pirklbauer, A.: What will occur after permafrost? Relevance of relict rock glaciers for the discharge behaviour of alpine catchments, Joannea – Geologie und Palaontologie, 12, 63–72, 2016.
- Zappa C. J., Jessup A. T., and Yeh H.: Skin layer recovery of free-surface wakes: Relationship to surface renewal and dependence on heat flux and background turbulence, Journal of Geophysical Research: Oceans, 103, 21711–21722, https://doi.org/10.1029/98JC01942, 1998.
- Zarroca, M., Roqué, C., Linares, R., Salminci, J. G., and Gutiérrez, F.: Natural acid rock drainage in alpine catchments: A side effect of climate warming, Science of The Total Environment, 778, 146070, https://doi.org/10.1016/j.scitotenv.2021.146070, 2021.
- Zierl, B. and Bugmann, H.: Global change impacts on hydrological processes in Alpine catchments, Water Resources Research, 41, https://doi.org/10.1029/2004WR003447, 2005.